Formation of the Nkob talc deposit by contact metamorphism and fluid infiltration into siliceous dolostones (Moroccan Anti-Atlas)

Adil Chatir, Julien Berger, Nasser Ennih, Antoine Triantafyllou, Philippe de Parseval, Ezzoura Errami, Hervé Diot, Jean-Marc Baele, Abdel Mohsine Aghzer, Christophe Monnier, et al.

Ore Geology Reviews 140 (2022) 104629

Contents lists available at ScienceDirect

Ore Geology Reviews

journal homepage: www.elsevier.com/locate/oregeorev

Formation of the Nkob talc deposit by contact metamorphism and fluid infiltration into siliceous dolostones (Moroccan Anti-Atlas)

Adil Chatir [a,b], Julien Berger [b,*], Nasser Ennih [a], Antoine Triantafyllou [c], Philippe de Parseval [b], Ezzoura Errami [a,d], Hervé Diot [e,f], Jean-Marc Baele [g], Abdel Mohsine Aghzer [a], Christophe Monnier [e], Mohammed Boutaleb [h]

[a] EGGPG, Département de Géologie, Faculté des Sciences, Université Chouaïb Doukkali, El Jadida Maroc
[b] Géosciences Environnement Toulouse (GET), Université de Toulouse, Observatoire Midi-Pyrénées, CNRS, IRD, UPS, Toulouse, France
[c] Laboratoire de Géologie de Lyon : Terre, Planètes et Environnement (LGL-TPE), Université Claude Bernard de Lyon 1, ENS de Lyon, France
[d] Got, Faculté Polydisciplinaire de Safi, Université Cadi Ayyad, Safi, Maroc
[e] Laboratoire de Planétologie et de Géodynamique LPG de Nantes, UMR-CNRS 6112, Université de Nantes, France
[f] Université de La Rochelle, La Rochelle, France
[g] Geology and Applied Geology Unit - Mining Geology, Université de Mons, 20, Place du Parc, B-7000, Belgium
[h] Consulting & Mining Development, Marrakech, Maroc

ARTICLE INFO

Keywords:
Pan-African
Marble
Serpentine
Skarn
Contact metamorphism
Hydrothermalism

ABSTRACT

The Nkob talc deposit located in the central Anti-Atlas Pan-African belt is hosted by magnesian and siliceous metacarbonates in the contact aureole of the Ediacaran Amassine granite. It consists of a stratified succession of green serpentine-rich marbles, black dolomitic marbles, talcitites and phlogopitites (variously retrogressed into chloritites) enclosed within andalusite metapelite hornfels and quartzites. Two main metamorphic stages have been defined for the formation of the marbles and talcitites: (1) high-temperature recrystallization occurred under amphibolite facies conditions (>500 °C). Temperature increase during granite emplacement led to the formation of forsterite, tremolite, phlogopite (±diopside) bearing assemblages in siliceous marbles and to transformation of dolomitic (calcite-free) marbles from pure dolostones. This high temperature stage is also characterized by the growth of andalusite porphyroblasts in the metapelites surrounding the deposit. (2) A low temperature retrograde hydrothermal stage characterized by the reactive infiltration of aqueous silica-rich fluid (presumably derived from the granitic body), in greenschist facies conditions (<520 °C). Hydrous silicate minerals, mostly serpentine and talc (+calcite), were formed during this stage within the rocks (after fluid infiltration along grain boundaries) or within veins (marking channeled fluid circulation). Talc in ores formed by two processes at Nkob: acicular talc near the granite formed after the breakdown of tremolite in a temperature range of 350 to 500 °C, while tabular talc in the external aureole formed via reaction between dolomite and siliceous-aqueous fluids in temperatures below 350 °C. The different types of marbles derive from pure to slightly siliceous dolomite but green and green-black marbles were strongly affected by interactions with siliceous-aqueous fluids forming serpentine-phlogopite veins with calcite reaction zones. The talcitite layers were also affected by similar hydrothermal H_2O-Si enrichment but their dolomitic precursor probably contained a more important detrital silicate fraction.

1. Introduction

Talc deposits are either associated with magnesian carbonate rocks (Blount & Vassiliou, 1980; Prochaska, 1989; Anderson et al., 1990; Prochaska et al., 1992; Hecht et al., 1999; Schandl et al., 1999; Tornos & Spiro, 2000; Shin & Lee, 2002) or with ultramafic units (El-Sharkawy, 2000; Tesalina et al., 2003). They can more rarely result from the diagenetic evolution of magnesian sediments (Noack et al., 1986; Tosca et al., 2011; Li et al. 2013). Several factors control the formation of talc such as the nature of the protolith, the fluid composition, pressure–temperature (P-T) conditions during its formation, as well as the occurrence, the density and the geometry of fractures acting as channels

* Corresponding author at: Géosciences Environnement Toulouse, 14 Avenue Edouard Belin, 31400 Toulouse, France.
E-mail address: julien.berger@get.omp.eu (J. Berger).

https://doi.org/10.1016/j.oregeorev.2021.104629
Received 13 July 2021; Received in revised form 29 November 2021; Accepted 30 November 2021
Available online 3 December 2021

for fluid circulation (Moine et al., 1989; Schandl et al., 2002; Bucher and Grapes, 2011; Wölfler et al., 2015). Talc mineralizations generally occur under relatively low metamorphic grade corresponding to the greenschist facies and require significant amounts of magnesium, silica, and H_2O, generally associated with decarbonatation reactions (Shin & Lee, 2002). The presence of Al, Ca or K in the host rocks generally tends to inhibit the formation of talc but favors the growth of other hydrous minerals such as phlogopite, chlorite and tremolite (Greenwood, 1998).

The Nkob talc deposit in the central Anti-Atlas belt of Morocco has been cited in the literature (Abia et al., 2011) but never studied, despite its potential as a large economic resource. Interestingly, the Nkob area is generally described as an ophiolitic complex (El-Boukhari, 1991; Thomas et al., 2002) due to the presence of metabasalts and metagabbros associated with small occurrences of serpentinites. In the same area, Thomas et al. (2002) also described a passive margin sequence containing dolomitic formations belonging to the Taghdout group.

This study aims at characterizing the geological setting of the Nkob talc deposits and to determine the evolution of pressure–temperature-XCO_2 conditions responsible for the growth of talc and its refinement. We present new geological maps, a detailed mineralogical characterization coupled to a thermodynamic modeling approach to propose a conceptual petrogenetic model of the Nkob talc formation that can be tested in similar deposits worldwide.

2. Geological setting

2.1. Regional setting

The Anti-Atlas orogen (Fig. 1) is a Neoproterozoic Pan-African belt bordering the northern edge of the West African craton (WAC); it formed during convergence between the latter and Avalonian terranes (Ennih and Liégeois, 2001; Gasquet et al., 2005; Ennih and Liégeois, 2008; Walsh et al., 2012; Blein et al., 2014; Hefferan et al., 2014; Soulaimani et al., 2018). Precambrian units are exposed in so-called "boutonnières" or inliers (=windows; Fig. 1b) within folded and faulted Paleozoic sedimentary series; the Nkob deposit belonging to the Sirwa inlier in central Anti-Atlas (Figs. 1 and 2). Paleoproterozoic rocks (schists, gneiss and granites of the Zenaga group; Thomas et al., 2004) making the cratonic basement crop out in western and central Anti-Atlas south and southwest of the Anti-Atlas Major Fault (AAMF; Fig. 1). They were affected by both the Eburnean (~2.0 Ga) and Pan-African (~630 Ma) orogenies. Sedimentary sequences and volcanic/subvolcanic basalts of the Taghdout group (Bouougri and Saquaque, 2004; Thomas et al., 2004; Fig. 2) are Late Paleoproterozoic to Neoproterozoic and probably formed during several rifting episodes (see Youbi et al., 2013; Ikenne et al., 2017; Bouougri et al., 2020). Supra-subduction ophiolites and oceanic arcs were active between 760 and 640 Ma and accreted onto the WAC margin probably between 640 and 620 Ma (Bou Azzer and Iriri groups; (Triantafyllou et al., 2016; Thomas et al., 2004; Samson et al., 2004; Triantafyllou et al., 2018, 2020; Hodel et al., 2020). The paroxysm of the Pan-African orogeny in the Anti-Atlas is evidenced by 620–600 Ma syn- to late-orogenic flysch basins associated with volcanic and volcano-sedimentary rocks (Fig. 2; Bou Salda and Saghro groups; Thomas et al., 2002; 2004; Ennih and Liégeois, 2008; Abati et al., 2010; Errami et al., 2020). The late Pan-African to Cadomian stages are marked by the production of huge volumes of magmas as early as 614 Ma (Assagrag suite) forming the thick Ouarzazate volcanic and volcano-sedimentary group (Figs. 1 and 2) and related plutons between 580 and 545 Ma (Thomas et al., 2002; Gasquet et al., 2005, 2008; Toummite et al., 2013; Errami et al., 2020). It is worth noting that the Anti-Atlas was subject to thick skin tectonics involving faulting and folding of Paleozoic series and reactivation of the Precambrian basement during the late Paleozoic Variscan orogeny (Burkhard et al., 2006). These long and repeated successions of igneous, hydrothermal and tectonic events from the Paleoproterozoic to the Late Paleozoic (and possibly the Triassic) generated numerous world class polymetallic deposits in the Anti-Atlas (see Tuduri et al., 2018 and reference therein).

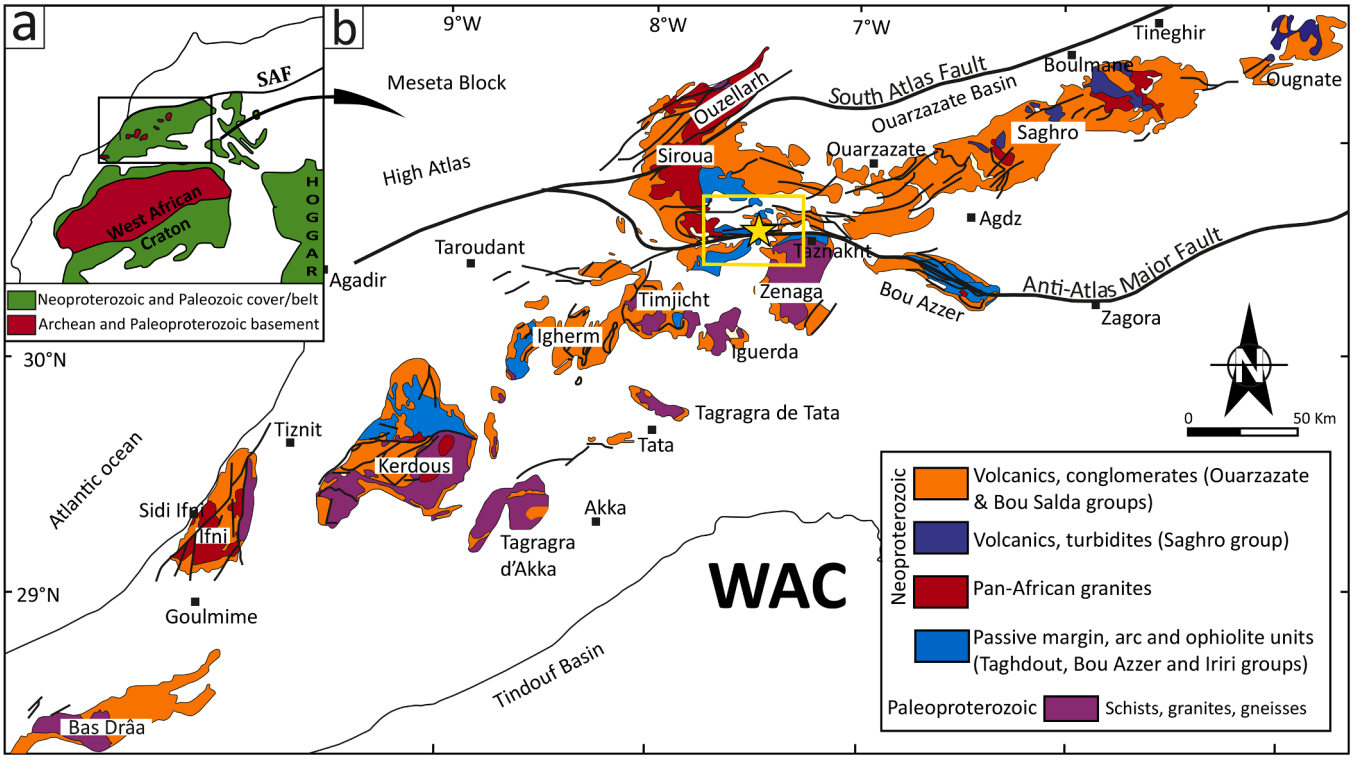

Fig. 1. (a) Location of the Anti-Atlas belt at the northern limit of the West African Craton (WAC). (b) Geological sketch map of the Anti-Atlas belt in southern Morocco showing the precambrian inliers (modified after Gasquet et al., 2008).

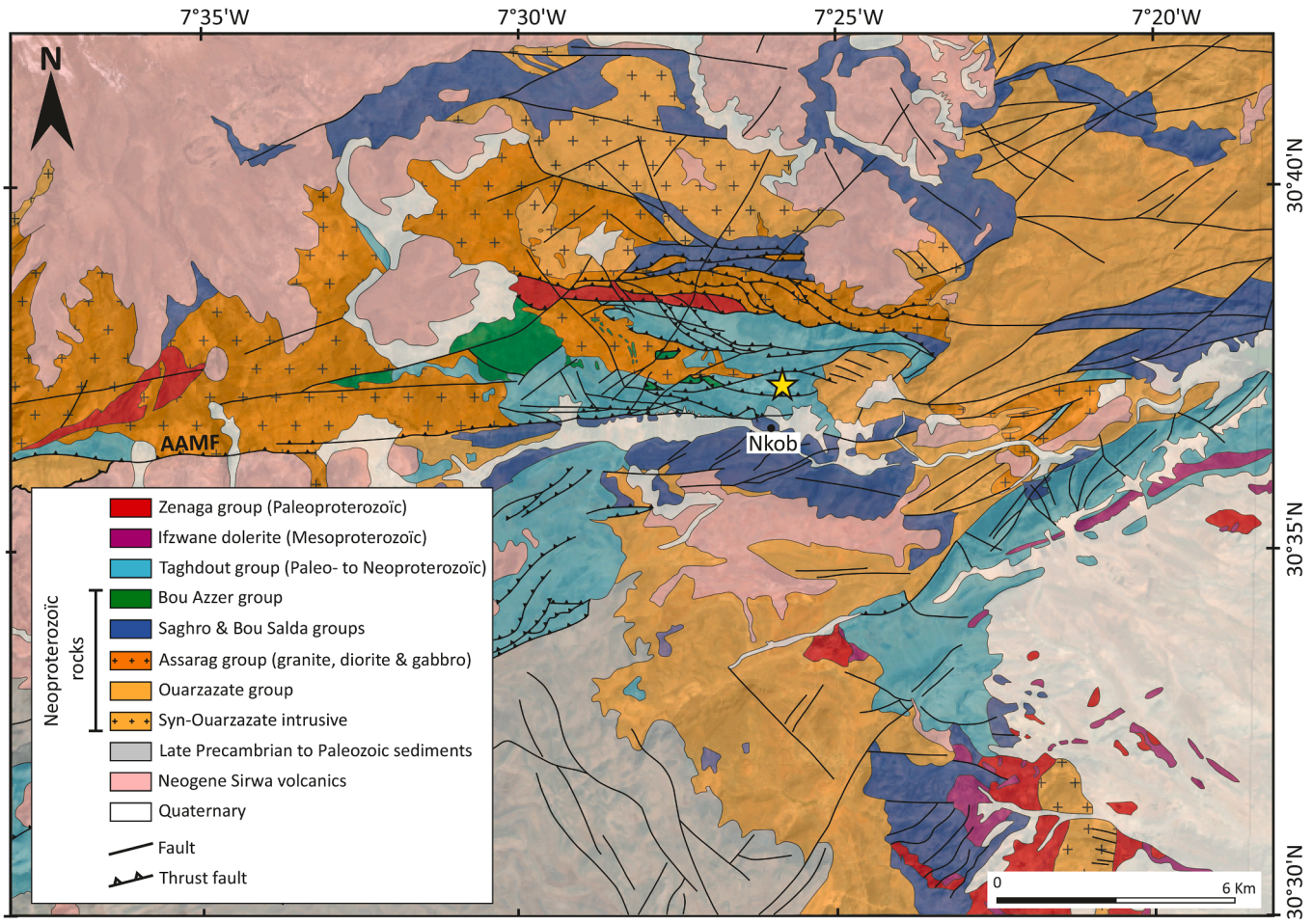

Fig. 2. Geological map of the southern part of the Siroua inlier (modified after Thomas et al., 2002). The star points to the location of the Nkob talc deposit. AAMF: Anti-Atlas Major Fault.

2.2. The Nkob talc deposit

The Nkob talc deposit formed in carbonated formation of the Taghdout group in the Sirwa inlier (Bouougri and Saquaque, 2004; Figs. 2 and 3). There, the Taghdout group consists of the following stratigraphic sequence (Figs. 3 and 4): (1) a thick sequence of altered basalts; (2) reddish quartz- and K-feldspar bearing (talc-absent) dolomitic rocks (3) two sequences of talc-bearing marbles associated with phlogopitites/chloritites and talcitites (described in detail below); (4) metapelitic units and metasandstones enclosing the main talc occurrence; (5) whitish quartzites locally showing tectonic brecciated textures. The structural position of the quartzite is unclear but they are systematically found within the metapelitic sequences near the contact with carbonate sequences. All these formations were subsequently intruded by the Amassine granite (614 ± 10 Ma; Thomas et al., 2002) also outcropping as small lenticular bodies within the talc-rich zone (Figs. 3 and 4). The age of the Taghdout is controversial, it was associated with the formation of a passive margin along the WAC during Early Neoproterozoic (Clauer, 1976; Cahen et al., 1984) but recent U-Pb dating on dolerite dykes, volcano-sedimentary layers and basaltic flows yielded Late Paleoproterozoic to Neoproterzoic ages (see Bouougri et al., 2020 for a recent review). Accordingly, dolomitic carbonates of the Taghdout group near Nkob deposited sometime between the Paleoproterozoic and the Cryogenian.

The talc deposit crops out over an area of approximately 2 × 0.5 km (Fig. 3) and consists of alternating beds of talcitites, marbles and phlogopitites/chloritites layers. It is enclosed within metapelites and metasandstones hornfels, in the contact aureole of the Amassine granitic pluton at its northwestern edge and it is covered by volcano-sedimentary rhyodacitic rocks of the Ouarzazate Group to the east (Figs. 4 and 5). Marbles are organized as metric to decametric beds, they appear black in the field (Fig. 6a) towards the east of the talc deposit, far from the granite, and turn green (Fig. 6b) close to the igneous intrusion. The transition between green and black marbles is progressive and is marked by marbles containing both black and green zones (Fig. 6c and 6d). Minor reddish marbles were found to the north of the deposit close to the granite intrusion. Talcitites are found as cm- to dm-thick beds alternating with marble layers. Two types have been identified: talcitite 1 (Fig. 6e) which is relatively compact and massive, located near the contact with the granitic body; and talcitite 2 (Fig. 6f) found far from the intrusion, which is more friable and marked by a pervasive foliation.. Relics of black marbles were found within the talcitite units in the south-east part of the deposit. Black phlogopitites and related green chloritites (Fig. 6g) form thin, cm-thick layers parallel to bedding within marbles or talcitites. They can be folded when present within a talc-rich layer. Small lenses of spotted metapelites (Fig. 6h) and metabasites were found within the deposit, generally along faults. A small and fresh dacitic dyke, presumably a feeder of the Ouarzazate group volcanics, cut across the marbles in the core of the deposit (Fig. 4).

The identification of a sequence of mappable isograds (meter- to centimeter-scale) within the deposit remains difficult. Only olivine and serpentine isograds have been identified. The presence of tremolite as an accessory phase often unidentifiable in the field, and the ubiquity of talc in the deposit do not allow their isograds to be traced at Nkob..

Sedimentary bedding is striking E-W and dipping to the north with variable values, generally ranging from 50 to 80° except near faults

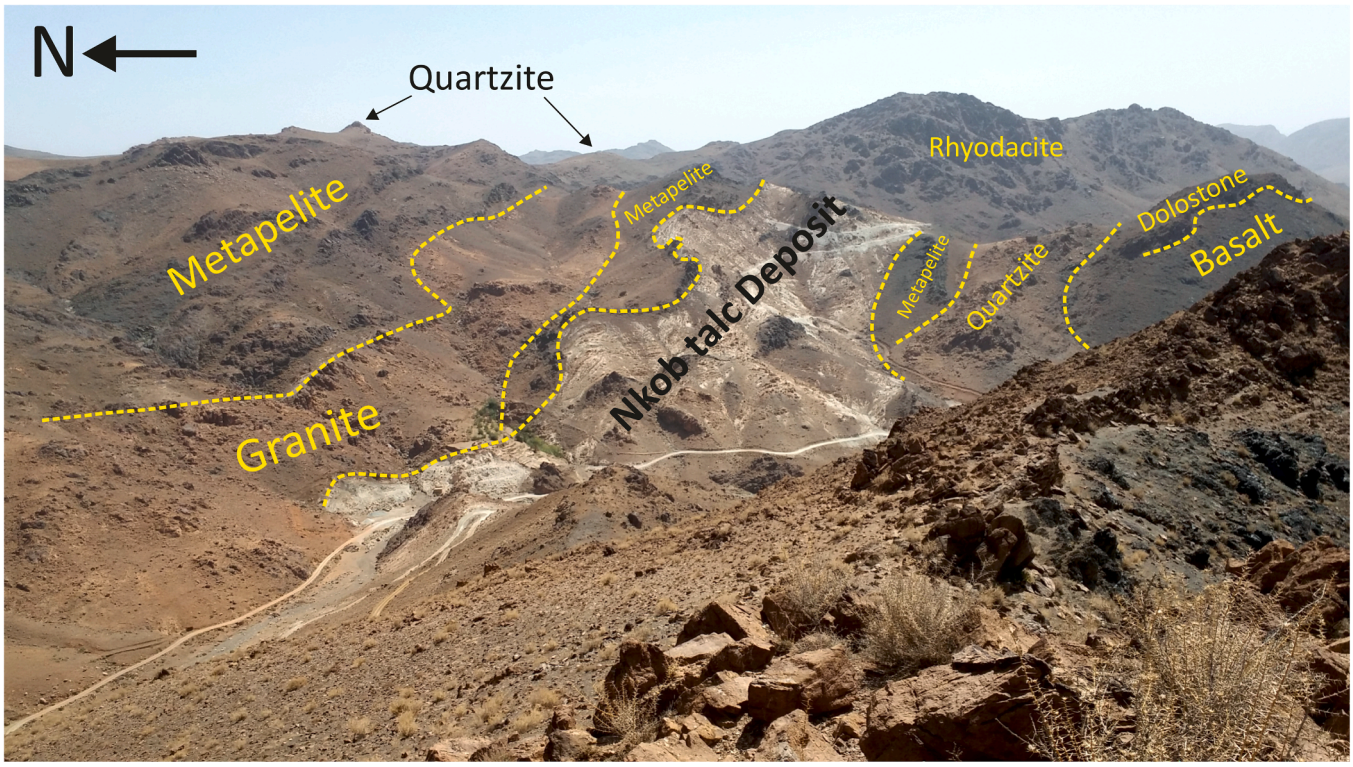

Fig. 3. Panoramic view of the Nkob talc deposit and surrounding rocks (the deposit reachs up to 300 m in thickness). It is intruded by the Amassine granite in the north and unconformably covered by the Ouarzazate volcanic group (rhyodacite) to the east. Note the presence of unmetamorphosed dolostone south of the deposit.

where lower values were measured (Fig. 4). Few anastomosing shear-zones showing S-C type fabric and implying dextral shearing were observed within the soft talc-rich layers. The C-planes are generally oriented WNW-ESE to NW-SE, while the S-planes are oriented NW-SE to E-W, both facing North. The talc deposit is also cut across by a dense network of steeply dipping strike-slip faults with an inverse component and subdivided into two main populations: N030 sinistral and N330 striking dextral (Fig. 4). At their contact bedding develops decametric vertical drag folds. Most of the faults are rooted within major E-W faults located south of the deposit and parallel to the transpressive sinistral Anti-Atlas major fault (Fig. 2).

Various veins were observed and their mineral assemblages vary with distance to the granite. Black marbles are cut across by greenish (serpentine-calcite-phlogopite) veins when close to the granite and white (tremolite-talc-calcite or talc-calcite) veins far from the intrusion. Other large white calcite veins cut across all units of the deposit, irrespective of their lithology and the distance from the granite. Millimetric chrysotile veins were only observed in green marbles west of the deposit, in contact with the intrusion. Some of the veins are deformed, commonly discontinuous, boudinaged and sometimes folded.

3. Sampling and analytical methods

Representative samples of dolostones, marbles, talcitites, phlogopitites and metapelites were selected for detailed mineralogical and petrological analysis. Samples were collected within and around the deposit to compare rocks affected by contact metamorphism to those showing no evidence for metamorphic recrystallization outside the aureole. Some representative samples are located on the map presented in Fig. 4 but the geographic coordinates of the 43 samples selected for this study are provided in the Appendix Table 1.Mineralogical analyses were performed by X-ray diffraction (XRD), scanning electron microscope (SEM) and electron microprobe (EMPA). XRD analysis (Fig. 7) were done on pulverized samples at the Geosciences Environment Toulouse (GET) laboratory and at the Department of Geology and Applied Geology, University of Mons (UMONS, Belgium). At GET, the diffraction measurements were carried out using a Bruker D2 diffractometer equipped with a curved position detector (CPS 120, Inel) covering an angle of 120°. At UMONS, bulk XRD analyses were conducted with a Bruker-Siemens D5000 diffractometer (Cu K-alpha radiation) set at 40 kV and 30 mA acceleration voltage and beam current, respectively. A rear graphite monochromator was used to minimize X-ray fluorescence from iron. The samples were dried and ground down to 50 μm and the resulting powder was manually pressed in XRD sample holders. The mounts were then X-rayed at 0.02°/s angular scan speed (2-theta) and 1.5 s counting time. The spectra were processed using Bruker-EVA software with JCPD PDF-2 powder diffraction database.

Polished thin-sections were examined by optical microscopy and with a JEOL JSM 6360LV SEM coupled to a Bruker EDX spectrometer (GET). Mineral composition (Table 1, Table 2 and Appendix Table A2) was determined at the «*Centre de micro-caractérisation Raimond Castaing*» (Toulouse, France) using a CAMECA SXFive electron microprobe. The operating conditions were: accelerating voltage 15 kV, beam current 10 or 20nA (depending on the mineral's resistance under the beam). Bulk rock major elements were dosed by ICP-OES after alkali fusion at the SARM (Nancy, France) following the digestion and analytical procedure described in Carignan et al. (2001).

4. Petrographic observations and mineral chemistry

4.1. Sedimentary and metasedimentary rocks

The Nkob talc deposit contains several lithotypes including: black, black-green, green and red marbles, talcitites and phlogopitites. These lithotypes alternate as regular, dm- to m-thick beds inherited from a former sedimentary sequence. Several generations of crosscutting veins were distinguished according to their mineralogical composition. Other lithologies crop out outside the talc deposit and consist of siliceous

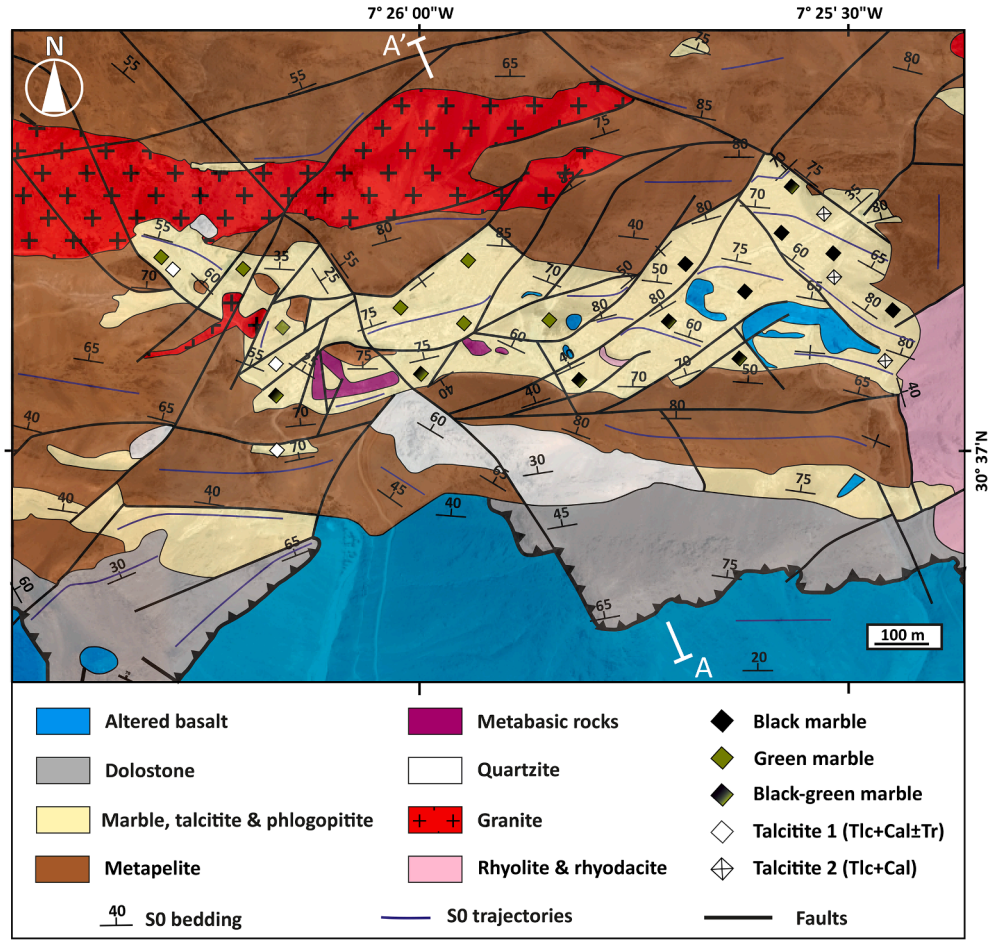

Fig. 4. New detailed geological map of the Nkob talc deposit. Trace of the cross section (Fig. 5) and location of some representative sampling sites (diamonds) are indicated.

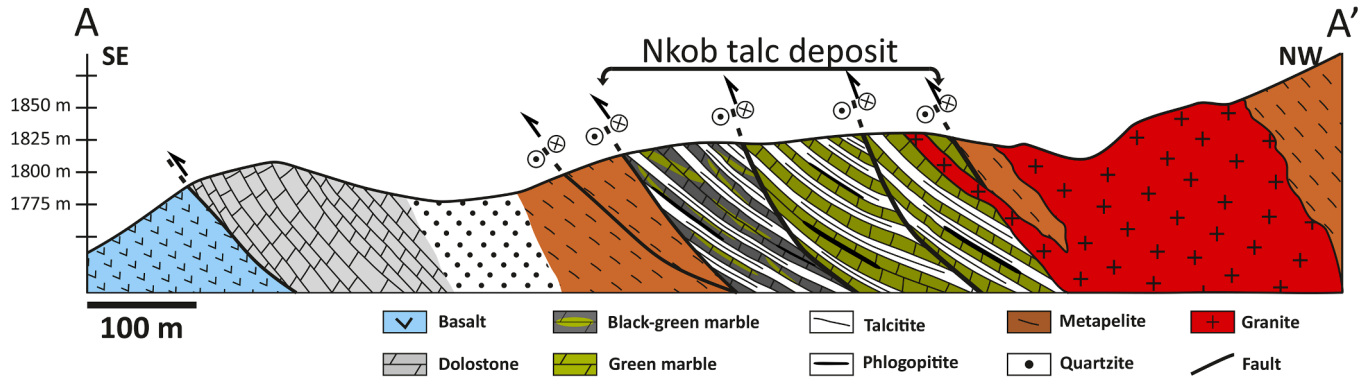

Fig. 5. N-S cross-section through the deposit, see location of the cross-section trace on Fig. 4.

dolostones and metapelites. Representative mineral chemical analyses are listed in Table 1 and Table 2.

Unmetamorphosed dolostone most likely represents the precursor of marbles and talcitites. They are dominated by dolomite (60–70 vol%) with variable amounts of quartz (5–30 vol%). In addition, iron oxides, K-feldspars and clays are found as accessory minerals (altogether < 10 vol%).

Black marbles (Fig. 6a) are chiefly made of dolomite (>70 vol%, with relatively high Fe contents ranging from 0.009 to 0.019 apfu) with calcite and small amounts of talc and chlorite flakes organized as a granoblastic texture with carbonate grains showing triple junctions. Talc crystals (>100 μm in length) occur as aggregates developing at carbonates grain boundaries where dolomite transforms to calcite (Fig. 8a). Phlogopite occurs as tabular crystals (up to 0.2 mm) intimately associated with serpentine and sometimes arranged as clusters partially to entirely replaced by chlorite (Fig. 8f). X_{Mg} in phlogopite ranges from 0.96 to 0.97 and Al content up to 1.76 apfu (Fig. 10c). Some of the phlogopite grains show a pronounced zoning in Ba with the rim being enriched in Ba and Al but depleted in K and Si and vice versa. Chlorite composition falls within the clinochlore field (Fig. 10d) with X_{Mg} ranges from 0.95 to 0.96 and Si between 3.40 and 3.63 (apfu).

Green marbles (Fig. 6b) occur in the vicinity of the granite intrusion.

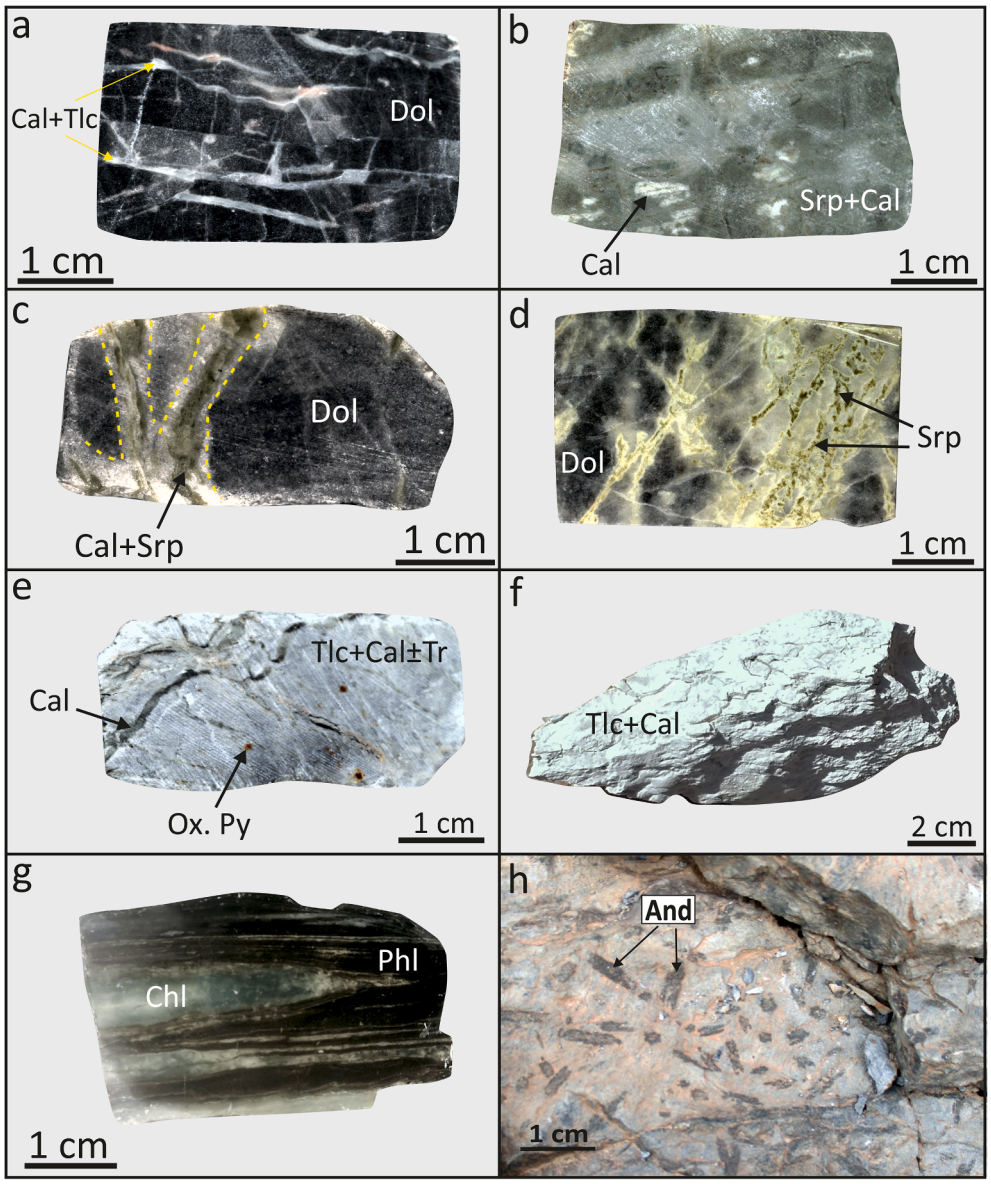

Fig. 6. Hand specimens and field photographs of samples from the Nkob deposit. (a) Section in a black dolomitic marble cut across by white calcite-talc veins. (b) Macroscopic view of green marble. (c) & (d) Calcite-serpentine veins cutting across black marble and forming black-green marble. (e) Hand-specimen of talcitite 1 (talc + calcite ± tremolite). (f) Macroscopic view of talcitite 2 (talc + calcite). (g) Hand-specimen of phlogopitite. Dark layers are phlogopite-rich while greenish light-coloured layers are chlorite-rich. (h) Andalusite metapelitic hornfel. Abbreviations: Cal: calcite, Dol: dolomite, Tlc: talc, Tr: tremolite, Ox. Py: oxidized pyrite, Srp: serpentine, Phl: phlogopite, Chl: chlorite, Ms: Muscovite, And: andalusite, Kfs: K-feldspar, Qz: quartz. (For interpretation of the references to colour in this figure legend, the reader is referred to the web version of this article.)

They show heteroblastic texture, mainly formed of serpentine (>50 vol %), calcite (approximately 35%) and small amounts of tremolite, talc, phlogopite, chlorite with rare olivine relics (Fig. 7). Serpentine can occur as veins associated to phlogopite with a calcite-rich reaction zone at the contact with host marbles (Fig. 6b). It is also present as large domains with a typical mesh texture, or as small isolated blebs into calcite containing rare relics of olivine (Fig. 8b, 8c and 8d) in the matrix of the marble. Si in serpentine is between 2.04 and 2.09 (apfu), for an X_{Mg} between 0.96 and 0.97. X_{Mg} in relictual olivine is slightly lower, around 0.93. Tremolite (100 μm) was observed as a minor component into large calcite grains. It forms needles or subhedral granular crystals commonly rimmed by talc (Fig. 8e). For talc, Si content varies between 3.98 and 4.00 (apfu), Mg values range from 2.78 to 2.84 (apfu), while the Al contents reach 0.11–0.12 (apfu; Fig. 10a). The presence of clinopyroxene is suggested by XRD analysis (Fig. 7) but this mineral was not observed in thin sections. Phlogopite occurs as tabular crystals (up to 0.2 mm) intimately associated with serpentine and is partially to completely replaced by chlorite (Fig. 8f). Chlorites are Mg-rich with X_{Mg} averaging around 0.96 (Fig. 10d) with variable Si contents between 3.62 and 3.87 (apfu). Disseminated euhedral grains of sulfides (i.e. pyrite, chalcopyrite) are found but often altered into iron oxides. According to their texture, they have crystallized after the main calcite-serpentine assemblages. Black-green marbles (Fig. 6c and d) are intermediate between the previously-described black and green marbles (Fig. 7). The green zones are serpentine-rich and form large masses in carbonates or as veins. Serpentine has almost the same composition that the one found in green marbles (Si : 2.03 and 2.11 apfu; X_{Mg} : 0.94 to 0.97).

The talcitites of the Nkob deposit (Fig. 6e,f) are characterized by a dominant talc-calcite association with minor chlorite, phlogopite and tremolite (Fig. 7). Two types of talc are identified according to their position in the deposit. Talc 1 (up to 100 μm), found in talcitites close to the contact with the granite, forms acicular and bladed aggregates and at the rim of tremolite (and rarely magnesio-hornblende) or within calcite suggesting that amphibole consumption led to talc growth (Fig. 9a and 9b). Talc 2, found in talcitites located far from the intrusion (south-eastern part of the deposit), shows large elongated grains (sometimes exceeding 100 μm) with a tabular habit, and which occur at calcite grain boundaries with a total absence of tremolite (Fig. 9c). Talc 1 and talc 2 are distinguished not only by their texture but also by their chemical composition (summarized in Fig. 10a and Table 2). Talc 1 is characterized by Si contents ranging from 4.01 to 4.05 (apfu) for Si contents between 4.02 and 4.06 for talc 2. Talc 1 is characterized by lower Fe

Table 1
Selected Electron Microprobe (EMP) analyses of Nkob deposit mineral phases.

Rock	Black marble	Black marble	Phlogopitite	Green marble	Black marbre	Green marble	Talcitite 2	Talcitite 1	Green marble	Green vein	Talcitite 1	Talcitite 1
Mineral	Phlogopite	Phlogopite	Phlogopite	Chlorite	Chlorite	Chlorite	Chlorite	Chlorite	Serpentine	Serpentine	Tremolite	Tremolite
Sample	DN38-C1-10	DN38-C2-7′	NK116-C1-3	DN43-C1-10	DN38-C2-30	DN43-C1-010	NK122-C1-33	TNC-C1-8	DN43-C2-032	DN03-C1-29	TNC-C1-12	TNC-C1-12
SiO_2 (wt %)	41.15	34.97	44.08	37.02	37.14	37.02	35.75	35.22	44.80	44.59	59.51	58.26
TiO_2	0.08	0.00	1.71	0.04	0.01	0.04	0.00	0.00	0.00	0.00	0.10	0.00
Al_2O_3	13.71	19.93	13.59	9.22	7.57	9.22	14.18	13.45	0.79	0.86	0.10	0.16
Cr_2O_3	0.00	0.00	0.03	0.02	0.02	0.02	0.03	0.02	0.01	0.00	0.01	0.00
FeO	1.51	1.59	4.11	2.09	3.29	2.09	4.05	1.80	2.03	3.03	1.03	0.89
MnO	0.01	0.04	0.04	0.00	0.00	0.00	0.02	0.01	0.00	0.00	0.09	0.00
MgO	28.14	23.57	21.03	30.41	37.82	30.41	30.63	34.30	38.81	39.27	23.76	23.64
CaO	0.00	0.00	0.10	4.29	0.72	4.29	0.04	0.04	0.12	0.09	13.65	13.99
Na_2O	0.03	0.24	0.08	0.02	0.00	0.02	0.00	0.00	0.00	0.00	0.08	0.00
K_2O	8.73	8.01	10.65	1.46	0.01	1.46	0.22	0.25	0.00	0.00	0.02	0.00
BaO	0.81	5.06	0.05	–	–	–	–	–	–	–	–	–
Total	94.96	94.07	96.98	84.84	86.63	84.84	85.44	85.53	86.80	88.46	98.59	96.93
Si (pfu)	2.91	2.62	3.10	3.62	3.52	3.62	3.43	3.35	2.08	2.06	8.03	7.99
Ti	0.00	0.00	0.09	0.00	0.00	0.00	0.00	0.00	0.00	0.00	0.01	0.00
Al	1.14	1.76	1.12	1.06	0.85	1.06	1.60	1.51	0.04	0.05	0.02	0.03
Cr	0.00	0.00	0.00	0.00	0.00	0.00	0.00	0.00	0.00	0.00	0.00	0.00
Fe	0.09	0.10	0.24	0.17	0.26	0.17	0.32	0.14	0.08	0.12	0.12	0.10
Mn	0.00	0.00	0.00	4.44	0.00	0.00	4.38	4.86	0.00	0.00	0.01	0.00
Mg	2.97	2.63	2.20	0.00	5.35	4.44	0.00	0.00	2.69	2.70	4.78	4.83
Ca	0.00	0.00	0.01	0.45	0.07	0.45	0.00	0.00	0.01	0.00	1.97	2.05
Na	0.00	0.03	0.01	0.00	0.00	0.00	0.00	0.00	0.00	0.00	0.02	0.00
K	0.79	0.76	0.95	0.18	0.00	0.18	0.03	0.03	0.00	0.00	0.00	0.00
Ba	0.06	0.36	0.00	–	–	–	–	–	–	–	–	–
XMg	0.97	0.96	0.90	0.96	0.95	0.96	0.93	0.97	0.97	0.96	0.98	0.98

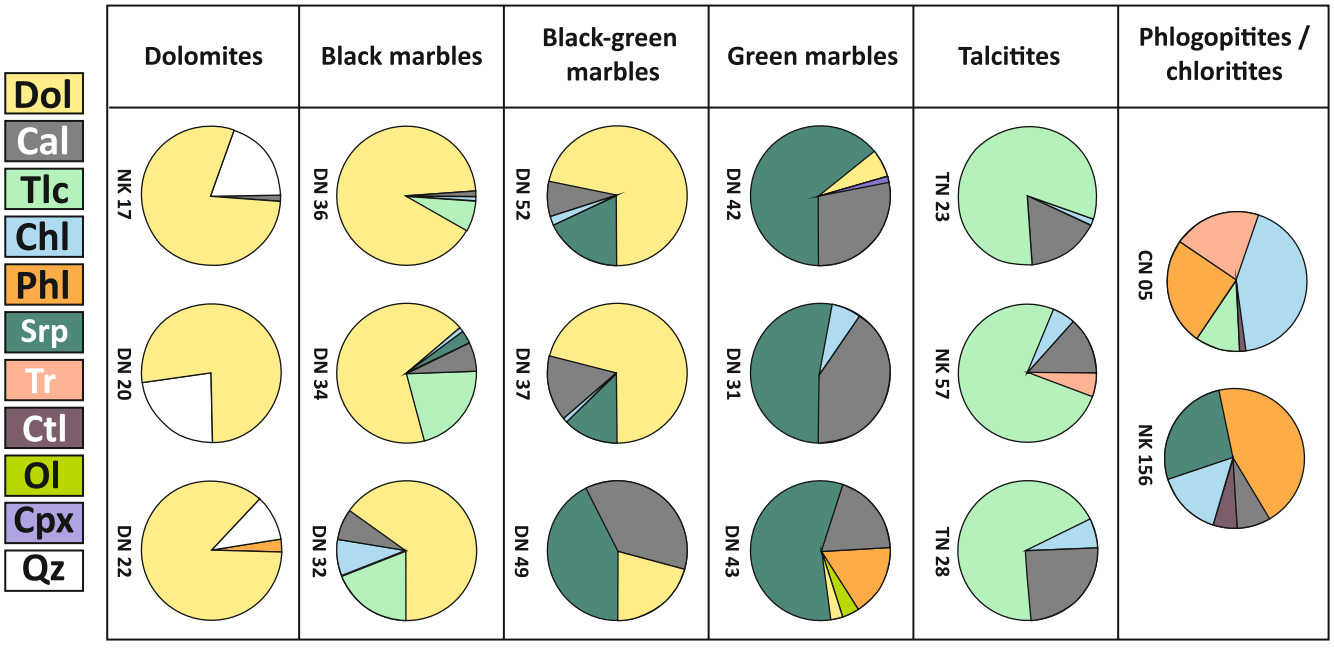

Fig. 7. Mineralogy of the different rocks of the Nkob deposit determined after XRD analysis. Abbreviations: Cal: calcite, Dol: dolomite, Tlc: talc, Srp: serpentine, Phl: phlogopite, Chl: chlorite, Ctl: chrysotile, Ol: olivine; Tr: tremolite; Qz: quartz.

(0.03 to 0.04 apfu) and higher Al (0.02–0.03 apfu), than talc 2, marked by higher Fe (0.06–0.07 apfu) and lower Al (0.00–0.02). A slight difference in X_{Mg} is observed between talc 1 (0.99) and talc 2 (0.98). Tremolite associated with talc 1 has Si content varying between 7.37 and 8.03 apfu and X_{Mg} around 0.97 and 0.98. Magnesian chlorites usually formed after phlogopite (rarely observed) are clinochlore (Fig. 9d) with X_{Mg} varying between 0.93 and 0.97, Si contents range from 3.28 to 3.39 apfu and Al values varying from 1.35 to 1.86 apfu (Fig. 10d). Few apatite grains (10–20 μm), zircon, rutile and iron oxides are present as accessory phases.

Phlogopitites (Fig. 6g) form black centimetric to decimetric layers alternating with marble beds. They are chiefly made of phlogopite with chlorite crystals, and talc (Fig. 9d). Compared to those in marbles, phlogopites are rich in Si (3.10–3.15 apfu), Ti (0.09–0.1) and K (0.95 apfu), and depleted in Mg (X_{Mg}: 0.90) (Fig. 10c). Chloritites formed by retrogression of phlogopitites and contain chlorite with minor amounts of tremolite and rare diopside (Si content : 2.01–2.03 apfu ; Ca contents :0.87–0.97; X_{Mg} = 0.88–0.93). Chlorites are Mg-rich (X_{Mg} = 0.96 ;

Table 2
Selected Electron Microprobe (EMP) analyses of talc in Nkob deposit rocks.

Rock	Green marble	Talcitite 1	Talcitite 1	Talcitite 2	Talcitite 2	Vein (Cal + Tlc)	Vein (Cal + Tr + Tlc)	Chloritites
Mineral	talc	talc	talc	talc	talc	talc	talc	talc
Sample	DN43-C1-07	TNC-C1-5	TNC-C1-19	NK122-C1-44	NK122-C1-64	DN03-C2-07	NK20-17	NK60-C01-17
SiO_2 (wt%)	62.72	63.49	63.77	62.36	63.05	64.52	61.96	62.87
TiO_2	0.00	0.00	0.00	0.00	0.00	0.00	0.00	0.06
Al_2O_3	1.42	0.39	0.34	0.29	0.06	0.17	0.53	0.69
Cr_2O_3	0.00	0.00	0.00	0.01	0.00	0.01	0.00	0.01
FeO	0.56	0.57	0.63	1.20	1.19	0.47	0.62	0.86
MnO	0.00	0.05	0.05	0.00	0.00	0.05	0.03	0.01
MgO	29.48	30.17	30.51	29.03	28.95	30.69	30.76	29.28
CaO	0.04	0.15	0.05	0.21	0.24	0.19	0.11	0.06
Na_2O	0.01	0.00	0.00	0.03	0.00	0.00	0.00	0.00
K_2O	0.01	0.09	0.06	0.05	0.00	0.01	0.00	0.09
Total	94.28	95.38	95.78	93.66	93.52	96.35	94.05	94.40
Si (pfu)	4.00	4.03	4.02	4.04	4.06	4.04	3.98	4.03
Ti	0.00	0.00	0.00	0.00	0.00	0.00	0.00	0.00
Al	0.11	0.03	0.02	0.02	0.00	0.01	0.04	0.05
Cr	0.00	0.00	0.00	0.00	0.00	0.00	0.00	0.00
Fe	0.03	0.03	0.03	0.07	0.06	0.02	0.03	0.05
Mn	0.00	0.00	0.00	0.00	0.00	0.00	0.00	0.00
Mg	2.80	2.85	2.87	2.80	2.78	2.86	2.94	2.80
Ca	0.00	0.01	0.00	0.01	0.02	0.01	0.01	0.00
Na	0.00	0.00	0.00	0.00	0.00	0.00	0.00	0.00
K	0.00	0.01	0.00	0.00	0.00	0.00	0.00	0.01
XMg	0.99	0.99	0.99	0.98	0.98	0.99	0.99	0.98

Fig. 10d) with relatively high Si (up to 3.67 apfu) and low Al (=1.20 apfu). Tremolite is present as elongated prismatic crystals scattered in the chloritized matrix with X_{Mg} above 0.95 and Si above 7.9 apfu (Fig. 10b). Randomly distributed, individual, or aggregated titanite (<20 μm), apatite (<10 μm) grains are systematically present but accessory.

Metapelites consist of a fine-grained groundmass of quartz, muscovite, biotite, plagioclase and k-feldspar with andalusite (chiastolite) porphyroblasts. Muscovite forms tabular crystals with biotite but also develops at the rim of andalusite. Both muscovite types show almost the same composition, with Si content generally low, of the order of 3.01 to 3.3 apfu and K content ranges between 1.55 and 1.85 apfu. Biotite Ti contents range between 0.05 and 0.19 apfu, while the X_{Fe} (molar Fe/(Fe + Mg) ratio) ranges from 0.47 and 0.59. Chlorite develops on biotite crystals and has Si contents ranging between 2.72 and 3.04 apfu, Fe contents ranging between 2.03 and 2.56 apfu. Plagioclase is accessory and very calcic (X_{An} : 0.96–0.99). Accessory tourmaline, rutile, zircon, monazite were observed.

4.2. Veins

Greenish veins (<0.5 cm) cut across the black marbles (leading to the formation of black-green and green marbles; Fig. 6c & 6d) and are the main components of green marbles. They are rich in serpentine with minor amounts of phlogopite retrogressed to chlorite. In most cases, serpentine with a typical mesh texture is rimmed by a 100–200 μm thick calcite reaction zone (Fig. 11a) at the contact with dolomitic marbles. Phlogopite occurs as inclusion in serpentine with relatively high Si content (2.90 apfu ; Fig. 10c) and low K content (0.72 apfu) and is retrogressed into magnesian chlorite.

White calcite-tremolite-talc veins cut across the black marbles in the outer aureole of the pluton (Fig. 6a). They are characterized by a calcite-tremolite-talc association (Fig. 11b) with acicular talc (<100 μm) developing on tremolite rims. Tremolite has acicular and fibrous habit with values of Si ranging from 7.66 to 7.98 (apfu), Mg ranging from 4.74 to 4.85 (apfu) and Fe ranging from 0.05 to 0.06 (apfu) (Fig. 10b).

White veins made of calcite and talc without tremolite but with rare dolomite and serpentine were found in the southeastern corner of the deposit. Talc occurs as elongated isolated crystals (>150 μm) along calcite grain boundaries (Fig. 11c) and has relatively high Si contents (4.03–4.07 apfu) with X_{Mg} values around 0.99. Millimetric chrysotile veins (<0.2 mm) are also frequent in the green marbles (Fig. 11d).

5. Whole-rock geochemistry

Whole-rock geochemistry of each lithotype described in previous sections (black, black/green and green marbles, talcitites, unmetamorphosed dolostones, metapelites) can be found in Table 3 and Fig. 12a and 12b. Two samples of unmetamorphosed dolostone collected at the south, but outside the talc deposit were analyzed as they probably represent the precursor of marbles and talcitites. One sample shows high levels of SiO_2 (15.13 wt%) in agreement with the presence of detrital quartz, the other has low SiO_2 content (1.98 wt%), both have low H_2O (<0.5 wt%) (Fig. 12a). The dolostones are slightly more calcic (25.69–35.80 wt% CaO) with respect to magnesium (15.02 – 17.07 wt% MgO) translating in molar Ca/(Mg + Ca) ratios above 0.5 (Fig. 12b). Black marble samples have low SiO_2 and H_2O contents (1.85–3.98 wt% and < 0.5 wt%, respectively) with variable MgO content (12.74 and 21.74 wt%) and a CaO range (between 29.6 and 39.18 wt%) similar to that of unmetamorphosed dolostones. Globally black marbles and sedimentary siliceous dolomite lie on a “detrital silicates trend” joining pure dolomite (0 wt% SiO2 and 0 wt% H_2O) and a detrital endmember here represented by Nkob andalusite metapelites (66–81 wt% SiO_2 with ~ 2 wt% H_2O). Compared to the black marbles, black-green marbles are enriched in SiO_2 (11.04–14.33 wt%) and H_2O (3.40–3.68 wt%) and depleted in CO_2 (28.45–32.60 wt%) (Fig. 12). The green marble sample has the highest concentrations in SiO_2 (25.99 wt%) and H_2O (6.96 wt%) reflecting the abundance of serpentine in veins and in the matrix (Fig. 12). They are by consequence more magnesian with Ca/(Ca + Mg) molar ratios below < 0.5. Al_2O_3 and K_2O were detected but at very low concentrations (0.69 wt% and 0.08%, respectively). Green and black green marbles lie on a “hydrothermal serpentine trend” joining pure dolostone to pure serpentine on Fig. 12a. Talcitites are more enriched in SiO_2, varying from 12.24 to 26.10 wt% and more calcic (30.52 and 43.29 wt% CaO) than the green marble sample. They also show high H_2O content (1.26 to 3.16 wt%) while CO_2 contents are relatively lower (23.88 to 31.87 wt%) than other lithotypes. The Al_2O_3 concentrations are relatively high (up to 2.39 wt%) probably due to the presence of detrital feldspars or clays in the sedimentary protolith. Interestingly, talcitites lie between the hydrothermal serpentine trend and the detrital silicate trend on Fig. 12a.

Metapelite samples show high SiO_2 contents (66.45 to 81.03 wt%;

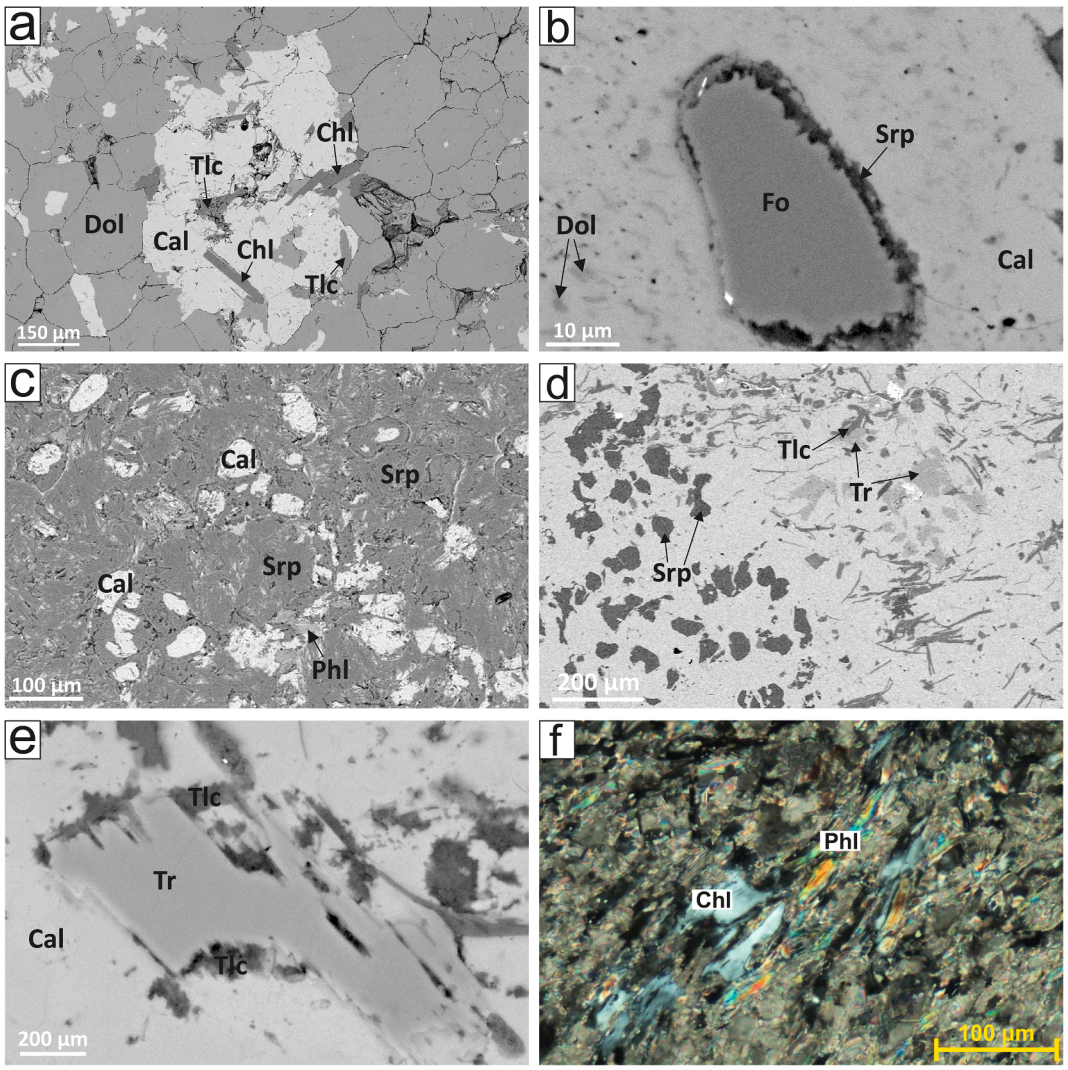

Fig. 8. Photomicrographs of marbles. (a) BSE image of black dolomitic marble showing calcite ± talc ± chlorite forming within pockets or at dolomite grain boundaries. (b) BSE image showing serpentinized olivine in green marble. (c) BSE image showing massive serpentine with calcite and phlogopite inclusions in green marble. (d) BSE image showing calcite-serpentine-tremolite ± talc association in green marble. (e) BSE image of talc rimming tremolite in green marble. (f) Crossed ploars optical image of chloritized phlogopite within green marble. Abbreviations: Cal: calcite, Dol: dolomite, Fo: forsterite, Tlc: talc, Srp: serpentine, Phl: phlogopite, Chl: chlorite, Tr: tremolite. (For interpretation of the references to colour in this figure legend, the reader is referred to the web version of this article.)

Fig. 12a) and low MgO contents (0.44–1.51 wt%) compared to marbles and siliceous dolostones. Their bulk composition varies from 10.19 to 18.4 wt% Al_2O_3, 0.7 to 2.73 wt% FeOtot and 0.43 to 0.69 wt% TiO_2. Alkali contents vary from 4.30 to 6.76 wt% of K_2O and from 0.06 to 0.26 wt% of Na_2O.

The Amassine granite samples have SiO_2 concentrations of 74–75 wt % and low CaO < 0.2 wt%. It classifies as a high K (K_2O: 4.5–5.6 wt%) slightly peraluminous granite (A/NK: 1.07; A/CNK: 1.04; Shand, 1927) comparable the Ediacaran high-K calc-alkaline granitoïds of the Sirwa inliers (see El Khanchaoui et al., 2001; Toummite et al., 2013).

6. Phase equilibrium calculations

A petrogenetic grid and several isochemical phase diagrams were constructed in order to constrain the P-T conditions of formation for the main mineralogical assemblages observed within the talc deposit. Pseudosections were built using the version 6.8.6 of Perple_X (Connolly, 1990, 2009) and thermodynamic database of Holland and Powell (2011). Solid solution models used for phase diagram calculations are Kf and San for alkali feldspar (Waldbaum and Thompson, 1968), oCcm(HP) for calcite (Anovitz and Essene, 1987), feldspar for plagioclase (Fuhrman and Lindsley, 1988), Cpx(HP) for clinopyroxene (Holland & Powell, 1996), O(HP) for olivine, Gt(HP) for garnet, Do(HP) for dolomite, Sp(HP) for spinel (Holland and Powell, 1998), Ilm(WPH) for ilmenite (White et al., 2001), cAmph(DP) for tremolite (Diener et al., 2007), Atg(PN) for serpentine (Padrón-Navarta et al., 2013), Opx(W) for orthopyroxene, Chl(W) for chlorite, Bi(W) for biotite and phlogopite, St (W) for staurolite, Crd(W) for cordierite, Mica(W) for muscovite (White et al., 2014).

Major minerals are carbonates and hydrous magnesian silicates with very low concentrations in Fe. We therefore started with a T-XCO_2 projection in the CaO-MgO-SiO_2-H_2O-CO_2 system (Fig. 13a and 13b) involving a saturated fluid phase containing variable amounts of CO_2 and H_2O (expressed as XCO_2, the molar $CO_2/(CO_2 + H_2O)$ ratio). The pressure was fixed at 2 kbar, a value coherent with the presence of andalusite in the metapelitic hornfels. It is worth noting that changing pressure (1, 2 or 3 kbar) has a very limited effect on the topology of the diagram (Fig. 13). The early olivine-calcite-dolomite assemblage found in green marble is stable above 540 °C. Serpentine forms by hydration of olivine or after a reaction involving tremolite and olivine at low temperatures (<520 °C) and low XCO_2 < 0.2. Tremolite is stable over a wide range of XCO_2 but only between 600 and 400 °C. It can form by

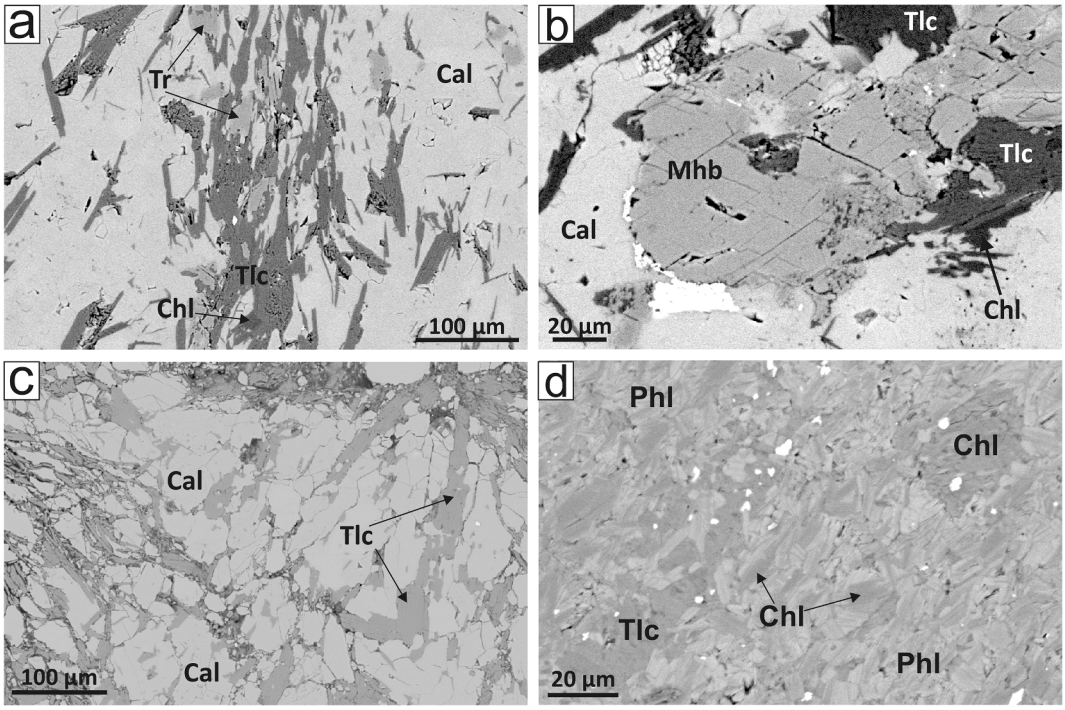

Fig. 9. BSE images of talcitites and phlogopitites. (a) Talc-calcite association within talcitite 1 near to the contact with the granite. Talc is acicular and contains some relics of tremolite. (b) Talc rimming an amphibole grain. (c) Talc-calcite association within talcitite 2 far from the granite. Talc has a tabular habit. (d) Phlogopitite dominated by phlogopite often altered to chlorite. Abbreviations: Cal: calcite, Dol: dolomite, Tlc: talc, Tr: tremolite, Mhb: magnesio-hornblende, Phl: phlogopite, Chl: chlorite.

destabilization of diopside (only found as an accessory phase after XRD analysis of green marbles). Talc occurs at lower temperatures and low CO_2 levels ($XCO_2 < 0.4$). The upper temperature limit for talc coincides with the lower limit for tremolite (~440 °C). An increase in temperature will replace the Dol + Qz assemblage with Tlc + Cal, while in the reverse retrograde path, a decrease in temperature will replace the Tr + Dol assemblage with Tlc + Cal. The late talc-calcite association of green marbles and talcitite is stable within a restricted range of temperatures (300–440 °C) and in equilibrium with aqueous fluids ($XCO_2 < 0.4$). Therefore, all mineral assemblages are in equilibrium with a hydrous fluid phase having low XCO_2 (<0.4).

The isochemical phase diagrams for marbles and talcitites were calculated using the bulk rock composition and fixed amounts of H_2O and CO_2 corresponding to those measured on the considered bulk rock (Table 3). Modal proportions were calculated and plotted on Fig. 15 to highlight the main reactions responsible for the formation of olivine, tremolite, talc and serpentine. Pressure was arbitrarily fixed at 2 kbar (in the andalusite stability field) but this parameter has only a limited effect on the variations of modal proportions with temperature

Metapelites were simulated with a saturated H_2O phase. The biotite-andalusite-K-feldspar-quartz-plagioclase assemblage observed in the metapelite is stable below 3.6 kbar in a narrow temperature range between 500 and 600 °C (Fig. 14a). Retrogression of andalusite into muscovite-rich clusters and transformation of biotite to chlorite both imply temperature conditions below 500 °C (Fig. 14a).

Black, dolomite-rich marbles are often devoid of hydrous silicate veins and were thus not or only slightly affected by hydrothermalism. The pseudosection for this bulk composition will thus give insights on the high temperature stage occurring before the development of hydrothermal fluid-rock interactions. Olivine forms at temperatures above 550 °C but above 650 °C at 2 kbar (Fig. 14b). With decreasing temperature, it reacts to form clinopyroxene and dolomite (Fig. 15a). Tremolite is stable below 600 °C (Fig. 14b) and forms after reaction between clinopyroxene and dolomite (Fig. 15a). Talc forms by a two steps retrogression of tremolite and dolomite producing also calcite around 500 and 370 °C (Fig. 14b, 15a).

The pseudosection calculated for a green marble (DN43) is presented in Fig. 15c and the evolution of modal proportion at 2 kbar in Fig. 15b. Green marbles represent rocks strongly affected by hydrothermal circulations resulting in the formation of abundant serpentine in veins or in the matrix. It is characterized by three successive assemblages including olivine - calcite - dolomite ± diopside ± phlogopite, serpentine - tremolite - calcite - dolomite ± phlogopite ± chlorite and talc - calcite - serpentine. Olivine (and minor clinopyroxene) within the green marbles attest for temperature above 450 °C (>500 °C at 2 kbar). Presence of tremolite and diopside in association with olivine, calcite and dolomite implies higher temperature, with a potential peak above 550 °C. Temperatures much above 550 °C are not expected because it would have produced large amounts of diopside while it is (<1 vol%) in green marbles. With temperature conditions decreasing below 500 °C (at 2 kbar), the phase diagram predicts the formation of antigorite and calcite by reaction of olivine, tremolite and dolomite (Fig. 14c, 15b). Finally, at around 350 °C, tremolite reacts with dolomite to produce retrograde talc and calcite (Fig. 15b). According to this calculation, the early, olivine-bearing assemblage formed above 500 °C, the main hydrothermal serpentine-calcite-tremolite-dolomite assemblage is in equilibrium between 500 and 350 °C while the talc-calcite intergrowths formed below 350 °C.

Bulk composition of sample NK132 was used to draw a pseudosection representative of talcitites (Fig. 14d) and the evolution of modal proportion with temperature at 2 kbar in Fig. 15c. Large amounts of diopside (up to 40 vol%, with olivine and calcite) are predicted above 550 °C (at 600 °C and 2 kbar) but were not observed. This indicates that either temperature never exceeded 600 °C or that diopside was completely retrogressed in our samples. Chlorite forms below 670 °C and reaches up to 13 vol% below 600 °C (Fig. 15c). Tremolite is a reaction product of pyroxene breakdown at 600 °C but its proportion decreases with the formation of Talc around 500 °C reaching about 10 vol% and is no more present below 350 °C Talc is stable with calcite as the dominant carbonate below 500 °C (Fig. 15c). They are both reaction

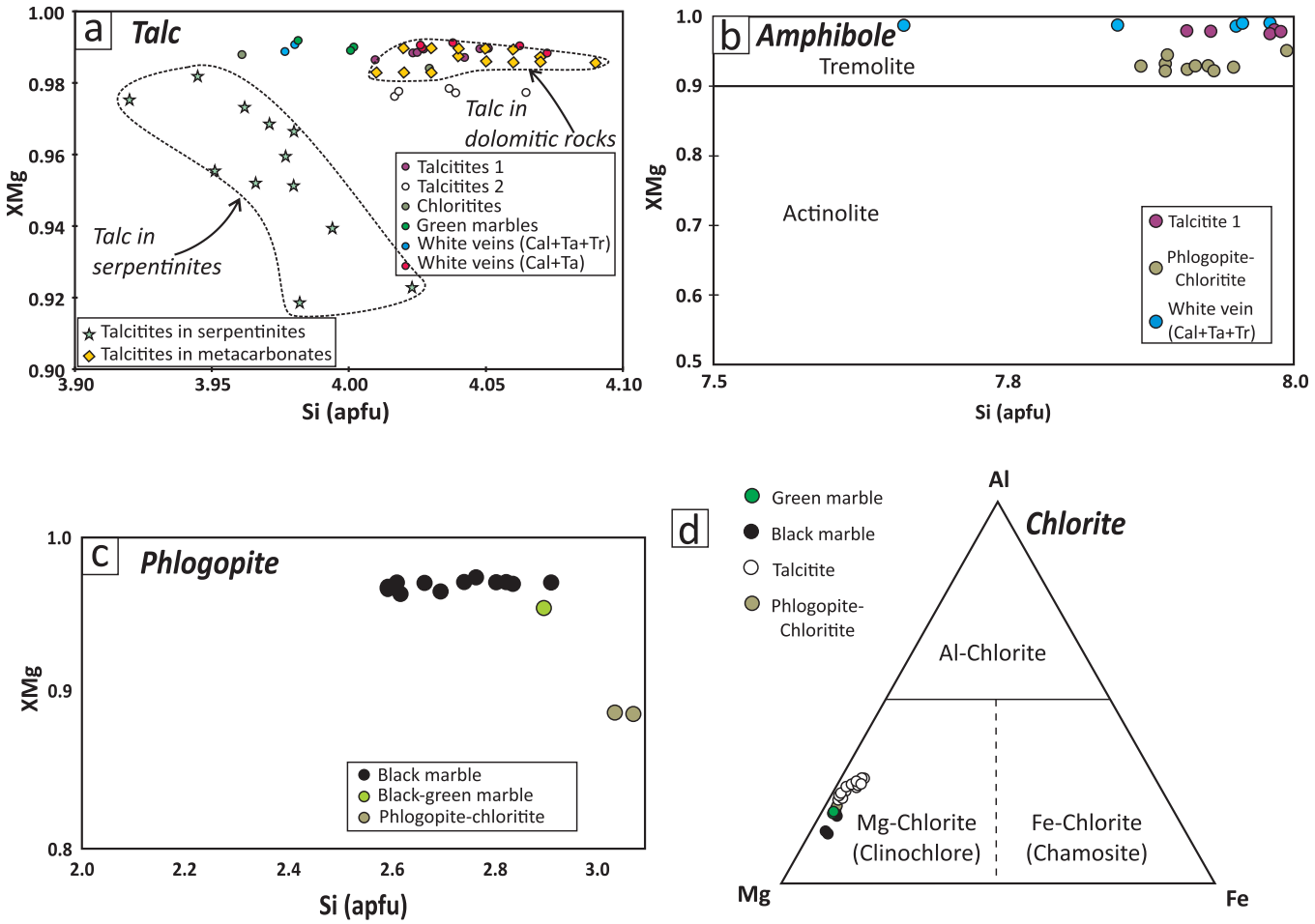

Fig. 10. Composition of some minerals in the Nkob deposit. (a) Si *versus* XMg diagram for talc (composition of talc in serpentinites after El-Sharkawy, 2000; talc hosted by carbonates from de Parseval, 1992). (b) Diagram of calcic amphibole classification after Leake et al. (1997). (c) Biotite classification diagram (after Rieder et al., 1999). (d) Chlorite classification diagram by Zane & Weiss (1998).

products of continuous tremolite-dolomite breakdown between 500 and 350 °C (Fig. 15c).

7. Discussion

7.1. Nature of protoliths and effect of fluid-rock interactions

Worldwide talc deposits are generally hosted in ultrabasic rocks (Simandl and Ogden, 1999; El-Sharkawy, 2000; Tesalina et al., 2003; Yalçin and Bozkaya, 2006) or magnesian metacarbonates (Blount & Vassiliou, 1980; Prochaska, 1989; Anderson et al., 1990; Prochaska et al., 1992; Schandl et al., 1999, 2002; Hecht et al., 1999; Tornos and Spiro, 2000; Shin & Lee, 2002; de Parseval et al., 2004; Wölfler et al., 2015; Tahir et al., 2018). Within the Nkob area, an allochthonous ophiolitic sequence is described as made of mafic rocks and ultramafic cumulates containing serpentine minerals such as antigorite and lizardite (El-Boukhari, 1991). The new geological map presented in Fig. 3, shows that the deposit is hosted by the dolomitic rocks of the Taghdout group, while talc has not yet been found in the ultramafic ophiolitic units located to the northwest of the studied area (Fig. 2). Dolomitic carbonates usually have higher bulk X_{Mg} (0.96–0.99; this study) than ophiolitic serpentinites from the Anti-Atlas (0.89–0.93; Hodel et al., 2020). Talc and serpentine in Nkob marbles and talcitites are consequently more magnesian than those formed in serpentinites (Fig. 10a).

Unmetamorphosed carbonated sequences in the Nkob and Taghdout areas are the most probable precursors of marbles and talcitites found in the deposit. Hence, sedimentary dolostones lie south of the deposit outside the 1 km-wide contact aureole surrounding the Amassine granite. Dolomitic carbonates exposed near the type locality of Taghdout (8 km east of Nkob) as well as those preserved near Nkob all contain detrital quartz, feldspar and clays (see Fig. 3). They locally display oolites and herringbone or cross bedding suggesting a tidal sedimentation environment. These carbonate sequences are the best local example of protoliths for metamorphic rocks now forming the Nkob talc deposit.

The origin of green marble (only found close to the granite) is directly linked to serpentine veins and development of calcite-hydrous magnesian silicates (serpentine, phlogopite, chlorite) assemblages along grain boundaries (Figs. 8 and 11). Away from the granite, only black marbles devoid of veins were found. Green serpentine-rich veins with their calcite reaction zones (Figs. 6 and 11a) increase in density toward the granite and control the formation of black-green marbles followed by green marbles near the granite. Moreover, the composition of green marbles does not correspond to any siliceous dolostone unaffected by veining nor metamorphism. Green marbles are rich in SiO_2 and H_2O and lie on a trend line joining pure serpentine and siliceous dolostone in the diagram in Fig. 12. The bulk composition of green and black-green marbles are thus strongly controlled by the reactive percolation of aqueous fluids enriched in dissolved silica forming serpentine-rich veins with calcite reactions zones and calcite with hydrous magnesian silicates within the rock (Figs. 8 and 11a) (Bucher-Nurminen, 1981; Bucher and Grapes, 2011). Hydrothermal serpentine characterizes many occurrences of magnesian marbles formed after contact metamorphism (i.e. Noh et al., 2020). The calcite-rich reaction zone in turn implies small-scale transfer of Mg from a carbonate (dolomite) to a silicate phase

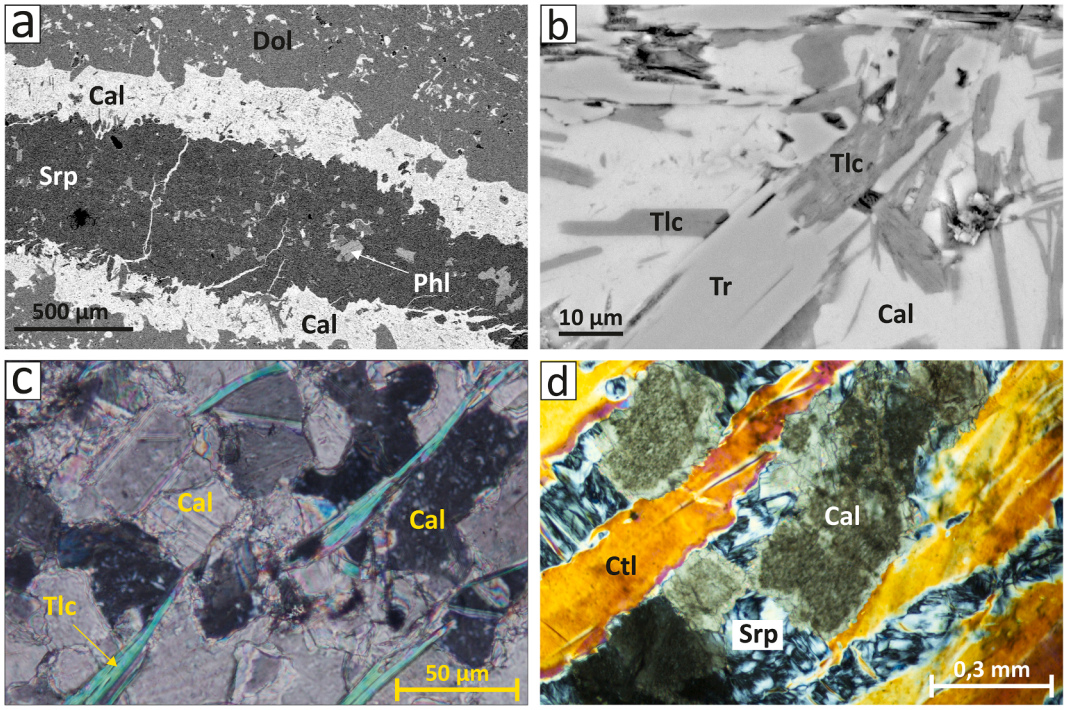

Fig. 11. Photomicrographs and back-scattered electron (BSE) images of veins from the deposit. (a) Serpentine ± phlogopite vein with calcite reaction zone cutting across the black marble. (b) White calcite-tremolite-talc vein cutting across black marble. Acicular and fibrous talc grows on tremolite rims. (c) White calcite-talc vein crosscutting black marble. Elongated talc is localized along calcite grain boundaries. (d) Chrysotile veins cutting across green marble. Abbreviations: Cal: calcite, Dol: dolomite; Tlc: talc, Srp: serpentine, Phl: phlogopite, Ctl: chrysotile. (For interpretation of the references to colour in this figure legend, the reader is referred to the web version of this article.)

(serpentine, phlogopite, chlorite) within the vein (Bucher-Nurminen, 1981). Isolated globule of serpentine in some green marbles (Fig. 8d) are however not compatible with an origin by fluid-rock interaction in veins. The presence of relict olivine in a few samples (Fig. 8b) argues that these globular serpentines formed after retrogressive hydration of olivine formed at high temperature (see following section) within the marbles.

Black dolomitic marbles have lower contents in silicate minerals compared to green marbles. Fluid infiltration was limited in these marbles and is only suggested by rare veins or by growth of calcite associated to hydrous magnesian silicates (serpentine, talc, chlorite, tremolite) along grains boundaries or in small millimetric pockets (Fig. 8a). From a geochemical point of view (Fig. 12), the composition of black marbles (and especially their low H_2O for variable SiO_2 contents) is close to unmetamorphosed dolostones and lie on a "detrital trend" in Fig. 12a. We therefore suggest that black marbles formed after near isochemical (except for H_2O and CO_2) metamorphism of siliceous dolostones.

Talcitites form decimetric to metric beds alternating with marbles. The bedding is inherited from the stratification of the sedimentary protolith. This observation suggests that protolith composition exerted a strong control on the formation of talcitites. Geochemically, the talcitites systematically plot between the "detrital" and the "serpentine vein" trend lines (Fig. 12a). Talcitites are consequently interpreted as former siliceous dolostones affected by infiltration of aqueous fluids. A similar interpretation was also proposed for other carbonate-hosted talc occurrences (Tahir et al., 2018).

We have not analyzed bedding-parallel phlogopitite layers due to their small size (thickness of several mm to cm) and the strong open-system retrogression into chloritites but by simple reasoning, we can assume that they are rich in K, Mg, Al, Si and H_2O. Such composition and structure (bedding-parallel layering and absence of contact reaction zones) would probably fit with former magnesian marls as thin layers separating carbonate beds. Phlogopitites are a common component in magnesian marbles formed after contact metamorphism, they are commonly interpreted as former thin sedimentary beds (see Bucher-Nurminen, 1988 for example). It is worth noting that most serpentine-rich veins also contain hydrothermal phlogopite (Fig. 11a) formed after reaction with hydrothermal fluid phase, indicating that the latter host significant amounts of K and probably Al.

7.2. *P-T-X conditions and the formation of talc at Nkob*

Petro-mineralogical investigations coupled with thermodynamic modeling suggest that the formation of the Nkob talc deposit is a multiple stages process controlled by the nature of the pre-metamorphic protoliths, the temperature conditions and the composition of the hydrothermal fluid phase. Two main stages can be defined for the formation of the talc deposit (and are summarized in Figs. 16 and 17): (1) a high-temperature stage related to the emplacement of the granitic body, followed by (2) a retrograde stage marked by intense rock-fluid interactions effective during the cooling of the intrusion and the host rocks.

The high-temperature stage ($T > 500$ °C) is defined by relict olivine (Fig. 8b), diopside and tremolite in green marbles outside veins and by andalusite-biotite association (Fig. 17a) in surrounding metapelitic hornfels. Olivine is stable above 450 °C in green marbles and above 550 °C in the composition representative of black marbles (Fig. 14) while the andalusite-biotite association is stable above 500 °C in Al-poor metapelites but below 3.5 kbar (Fig. 14). High thermal gradient (>50 °C/km), concentric disposition of mineral assemblages around the granite (Fig. 3) and the absence of deformation during metamorphism can only be explained by contact metamorphism during granite intrusion around ca 614 Ma (Thomas et al., 2002). Siliceous dolostones in contact with the igneous intrusion were transformed into marbles containing (Figs. 14 and 15): calcite + dolomite + forsterite + phlogopite ± diopside, while protoliths with a more calcic composition were transformed into marbles with mineral assemblage: calcite + dolomite +

Table 3
Bulk rock major element contents of representative rocks from the deposit.

Samples	NK 51	DN 20	DN 36	DN 40	DN 38	DN 49	DN 43	NK 132	TN 24	TN 36	NK 44	MN 01	NK 120	MZ 01	MZ 04
Lithology	Dolostone	Dolostone	Black marble	Black marble	Black-green marble	Black-green marble	Green marble	Talcitite	Talcitite	Talcitite	Metapelite	Metapelite	Metapelite	Granite	Granite
SiO_2 (wt%)	1.98	15.13	1.85	3.98	14.33	11.04	25.99	18.74	24.47	26.10	66.45	72.10	81.03	75.13	74.04
TiO_2	< LOD	< LOD	< LOD	< LOD	0.13	< LOD	0.02	0.06	0.02	0.02	0.69	0.64	0.43	0.18	0.16
Al_2O_3	0.54	0.22	0.28	0.39	3.59	0.66	0.69	2.39	0.62	0.71	18.41	15.52	10.19	13.21	12.39
FeOtot	0.89	0.64	0.60	0.52	1.17	0.72	1.32	0.55	0.57	0.71	2.73	1.49	0.70	0.62	2.09
MnO	0.22	0.53	0.06	0.12	0.08	0.09	0.05	0.07	0.04	0.05	< LOD	< LOD	< LOD	< LOD	< LOD
MgO	15.02	17.07	21.24	12.74	15.88	10.72	23.61	12.30	12.62	13.82	1.51	0.98	0.44	0.19	0.10
CaO	35.80	25.69	29.60	39.18	31.23	40.27	21.98	34.34	32.18	30.52	0.13	0.11	0.08	0.20	0.15
Na_2O	< LOD	0.03	< LOD	< LOD	< LOD	< LOD	< LOD	< LOD	0.04	0.05	0.26	0.13	0.06	4.50	3.39
K_2O	< LOD	0.07	< LOD	< LOD	0.78	< LOD	0.08	< LOD	0.22	0.04	6.76	5.35	4.30	4.53	5.58
P_2O_5	< LOD	< LOD	< LOD	< LOD	< LOD	< LOD	< LOD	< LOD	< LOD	0.10	< LOD	< LOD	< LOD	< LOD	< LOD
LOI	44.22	39.43	45.11	41.99	32.04	35.41	25.38	30.25	27.98	27.00	2.76	2.81	2.78	0.81	0.76
Total	98.76	98.87	98.80	98.97	99.34	98.97	99.26	98.76	98.83	99.19	100.01	99.29	100.08	99.45	98.90
H_2O total	0.48	0.31	0.35	0.67	3.68	3.40	6.96	3.16	2.37	2.72	0.00	0.00	0.00	0.00	0.00
CO_2 total	42.75	38.88	42.08	42.24	28.45	32.60	19.15	27.45	25.15	23.88					

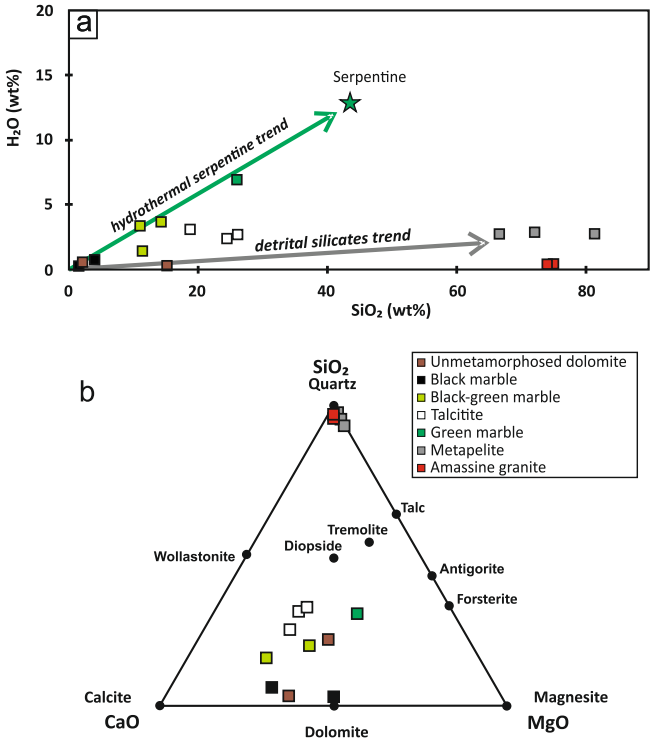

Fig. 12. a) Variation diagrams of SiO_2 vs H_2O measured in bulk rocks of the deposit. The green star represents pure Mg-serpentine composition. b) Molar CaO-MgO-SiO_2 ($+H_2O$ + CO_2) ternary diagram showing the bulk chemical compositions and main minerals of the rocks investigated in this study. (For interpretation of the references to colour in this figure legend, the reader is referred to the web version of this article.)

tremolite + phlogopite. Such assemblages are commonly described in contact aureole involving impure dolostones where temperature reached amphibolite facies conditions near the intrusion (Rice, 1977; Holness, 1997; Noh et al., 2020).

The hydrothermal retrograde stage (T°<520 °C) is defined by the formation of hydrous silicate phases (serpentine, chlorite, talc) and calcite overprinting high-temperature assemblages crystallized in veins and within the rocks along grain boundaries (Fig. 17b). Serpentine formed below 520 °C (Fig. 14) while talc is stable below 350 °C in green marbles and below 500 °C in talcitites. This event requires the introduction of H_2O-Si fluids (probably derived from the granite) to account for the following replacement of olivine by serpentine, talc crystallization after tremolite and chlorite after phlogopite (Fig. 17b). As the minerals in veins (serpentine-calcite-phlogopite ± talc) are similar to assemblages characterizing the hydrothermal retrograde stage, we suggest that reactive fluid infiltration occurred below 500 °C, during retrogression. Calculated modal proportion during temperature decrease at a fixed pressure (here fixed at 2 kbar; Fig. 15) show that olivine reacts with dolomite and tremolite to form calcite and antigorite in marbles (500–530 °C in Fig. 15a).

As suggested by talcitite bulk composition (Fig. 12a), infiltration of the fluids into marbles containing tremolite, led to the formation of calcite + talc assemblage after tremolite + dolomite according to the reaction (1) at a temperature around 350–500 °C (Figs. 14 and 15). This explains the formation of acicular talc in talcitites 1 preserving some relics of tremolite (Fig. 6e and 9a). The following retrograde reaction (not equilibrated) can be suggested following the results presented in Fig. 15b:

$$Tr + Dol + H_2O \rightarrow Tlc + Cal + Srp \quad (1)$$

Shin and Lee (2002) also proposed that tremolite destabilize to form talc between 380 and 400 °C, but with associated loss of Mg and gain of

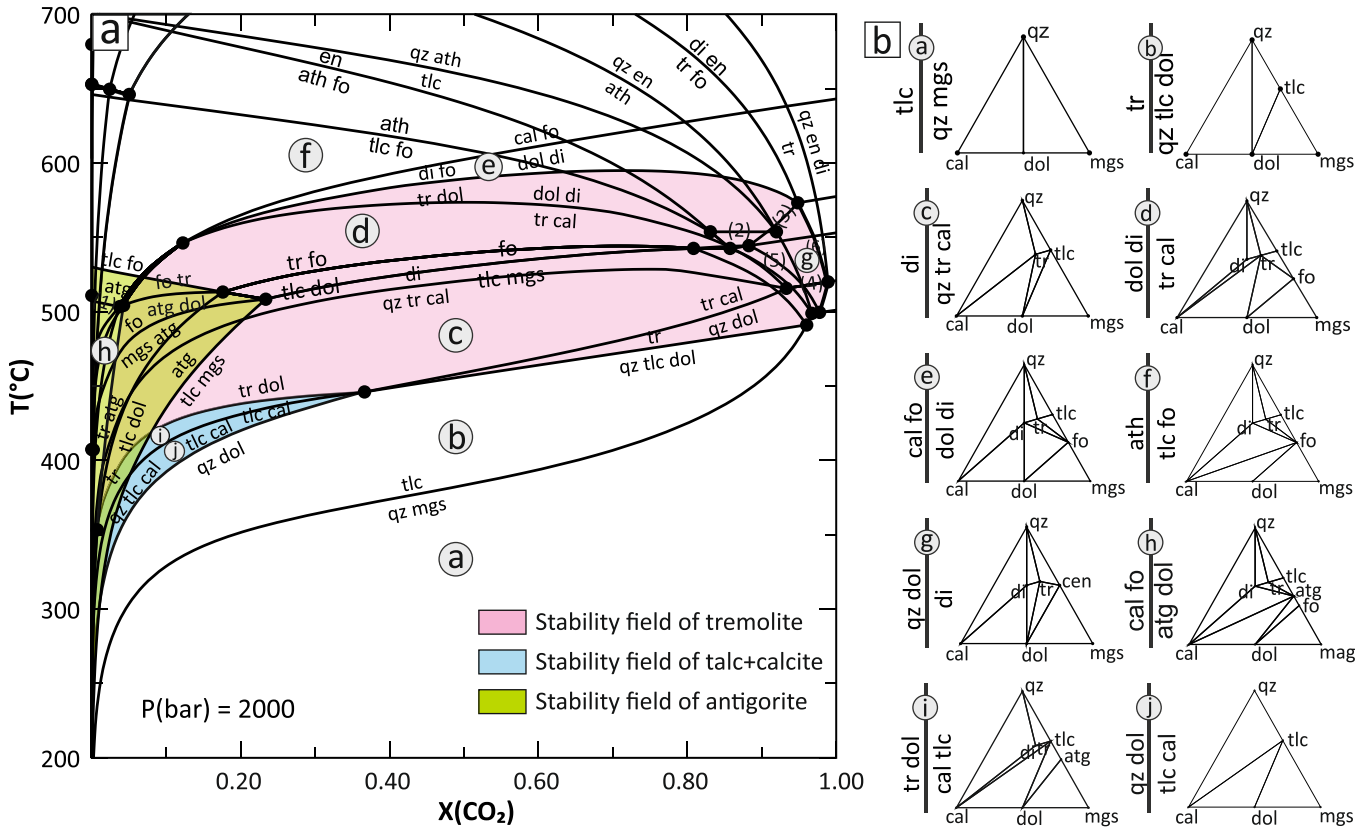

Fig. 13. (a) T-XCO_2 phase diagram in the system of CaO-MgO-SiO_2-H_2O-CO_2 at P = 2 kbar. Reactions indicated by numbered curves are as follows: (1) di atg = fo tr; (2) en tlc = ath; (3) dol en = fo tr; (4) qz dol = di; (5) mgs tr = dol en; (6) dol tr = en di. (b) Phase compatibility diagrams showing the potential mineral assemblages in some representative fields of Fig. 13a. All mineral abbreviations are after Whitney and Evans (2010).

Ca during hydrothermal reaction.

Distal from the granitic body tremolite was never observed and talc has a tabular habit. This probably argues that talcitites 2 (those with tabular talc) never reached the stability field of tremolite and were formed at temperature below 350 °C (Fig. 14c). We suggest that this tabular talc forms by reaction between dolomite and silica-rich hydrous fluids and/or detrital quartz in the presence of H_2O to form talc according to the following reaction (Skippen, 1971):

$$\mathrm{Dol} + 4\,\mathrm{SiO_2} + \mathrm{H_2O} \rightarrow \mathrm{Tlc} + 3\,\mathrm{Cal} + 3\,\mathrm{CO_2} \quad (2)$$

The latter is often proposed to form talc by prograde hydrothermal reaction involving either SiO_2 from quartz or in an aqueous fluid, although the speciation of some elements required in the structure of talc (Si, Mg, H) is sometimes different (Shin and Lee, 2003; de Parseval et al., 2004). In the case of Nkob, quartz is observed in the barren, unmetamorphosed dolostone, suggesting that SiO_2 necessary to form Talc was already present in the precursor. Nevertheless, the SiO_2 and H_2O contents of talcitite are too high compared to unmetamorphosed dolomite (Fig. 12a), suggesting that these rocks were pervasively transformed hydrothermal circulation that resulted in extra input of SiO_2 and H_2O.

The mineralogical composition of green veins formed during the retrograde hydrothermal stage and the information gathered with T-XCO_2 sections suggest that fluids reacting with the rocks where mostly hydrous, with XCO_2 below 0.4 (presumably 0.2; Fig. 13) and high dissolved Si contents. Fluid inclusion were observed in some calcite crystals associated with green serpentine veins, but their size (<30 μm and most often around 10 μm) do not allow to perform a microthermometry-based determination of their composition.

The very late, low temperature hydrothermal overprint is responsible for the formation of chlorite after phlogopite (Yau and Nakatani, 1984; Chabu, 1995; Sinaei-Esfahani, 2013), the crystallization of iron sulphides and oxides, as well as the formation of chrysotile veins.

7.3. Comparison with other talc deposits

Nkob belongs to the class of carbonate-hosted deposits formed in the contact aureole of a silicic pluton (Fig. 3). Transformation of dolostone into marble occurred by heat transfer from the pluton to the host sedimentary series and by infiltration of H_2O-Si-rich fluids most probably derived from the cooling granite. Silicon needed to form magnesian silicates in marbles originates both from a detrital silicate fraction within the dolomitic precursor but also by addition of external Si during hydrothermalism (Fig. 12a) as it is classically proposed in similar context worldwide (Anderson et al., 1990; Bucher and Grapes, 2011; Schandl et al., 1999; Cook and Bowman, 2000; Shin and Lee, 2002; Tahir et al., 2018). Temperatures needed to form olivine in marble not affected by hydrotermalism near the granite are around 450–600 °C (Fig. 14). Talc 1 formed by retrogression of tremolite around 350–500 °C (Fig. 15) while talc 2 probably formed by reaction between dolomite and aqueous Si-rich fluids at temperature < 350 °C (Fig. 15). These characteristics are very comparable to talc deposits formed from carbonates within a contact aureole, especially the Korean, Egypt and Afghanistan occurrences (Schandl et al., 1999; Shin and Lee, 2002; Tahir et al., 2018) where tremolite is involved in the generation of talc during retrogression and hydrothermalism of calc-silicate rocks. However, the absence of calc-silicate rocks (Ca-Si rich rocks, often rich in diopside, tremolite with accessory wollastonite) in Nkob is at variance with the occurrences studied by Shin and Lee (2002). Maximum SiO_2 content in marbles and talcitite from Nkob are below 26 wt% while it reaches up to 56% in South Korean occurrences (Shin and Lee, 2002). In this latter case study, the authors interpreted the calc-silicate rocks as a product of

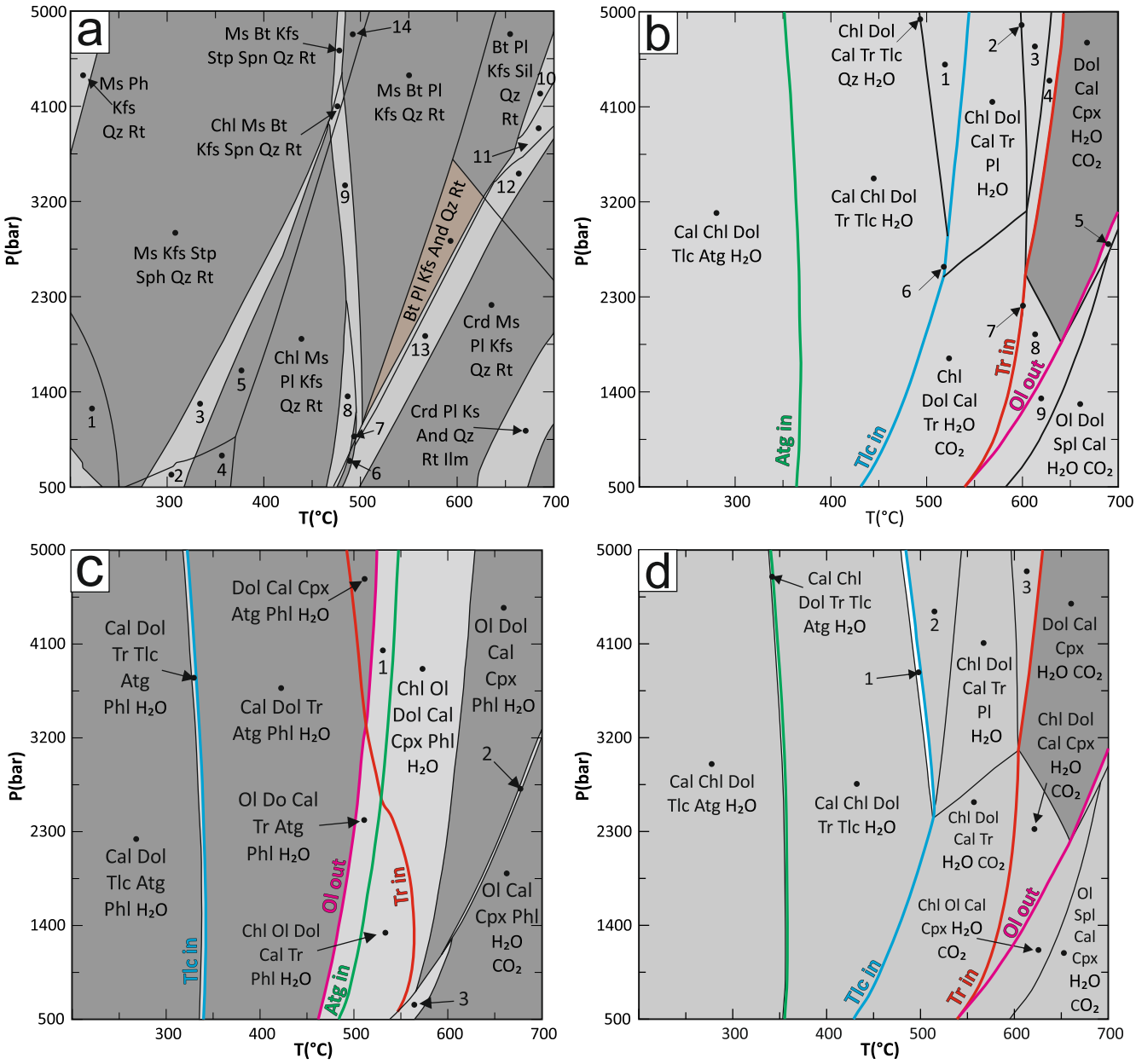

Fig. 14. P-T pseudosections calculated with Perple_X using bulk composition for Nkob deposit rocks. Pseudosections were calculated with fixed amounts of H_2O and CO_2 except for the metapelites for which H_2O is considered in excess. (a) pseudosections calculated with Perplex_ program using bulk composition for a metapelite from Nkob (sample NK44). The peak metamorphic assemblage field is shaded in orange. (b) P-T pseudosection calculated for a black marble (sample DN40). (c) P–T pseudosection calculated for a green marble (sample DN43). (d) P–T pseudosection calculated for a talcitite (sample NK113). All mineral abbreviations are after Whitney and Evans (2010). (For interpretation of the references to colour in this figure legend, the reader is referred to the web version of this article.)

decarbonation and Si-metasomatism from the original dolomite during the prograde stage. At Nkob silicification and decarbonation were not observed during the prograde stage, addition of Si (and H_2O) occurred during retrograde hydrothermalism and led to the formation of serpentine + phlogopite veins with calcite reactions zones (Fig. 11a) at temperature < 520 °C (the upper boundary for stability of serpentine) but also replacement of dolomite by calcite and hydrous magnesian silicates along grain boundaries (Fig. 8a).

Many talc deposits are linked to the development of faults or shear zones concomitant with hydrotermalism, as for example at Trimouns in France (de Parseval et al., 2004), Lassing and Rabenwald in Germany (Prochaska, 1989); Göpfersgrün in Germany (Hecht et al., 1999) and Puebla de Lillo in Spain (Torros and Spiro, 2000). These deposits usually record lower temperature of metamorphism/hydrothermalism (generally < 400 °C; Hecht et al., 1999; Moine et al., 1989), which, however, can reach up to 550 °C when formed at higher pressure (up to 9 kbar; Moine et al., 1989). The mineralogy of these deposits is also quite different. Tremolite and serpentine are rare or absent while chlorite is generally a very abundant mineral associated with talc (Prochaska, 1989; Moine et al., 1989; de Parseval et al., 2004). At Nkob, chlorite is common but rather as minor component and most often related to the retrogression of phlogopite. These major differences are the consequences of metasomatic processes exerting a major control on talc deposits linked to faults or shear zones and to the presence of aluminous schists near the channels localizing hydrothermal circulations. For example, the Trimouns talc and chlorite ores formed during a rifting episode where high geothermal gradient combined to active tectonics triggered/enhanced fluid circulation and put into contact micaschists, schists and magnesian carbonates. Talc formed after metasomatic transformation of dolomitic carbonates while aluminous schists

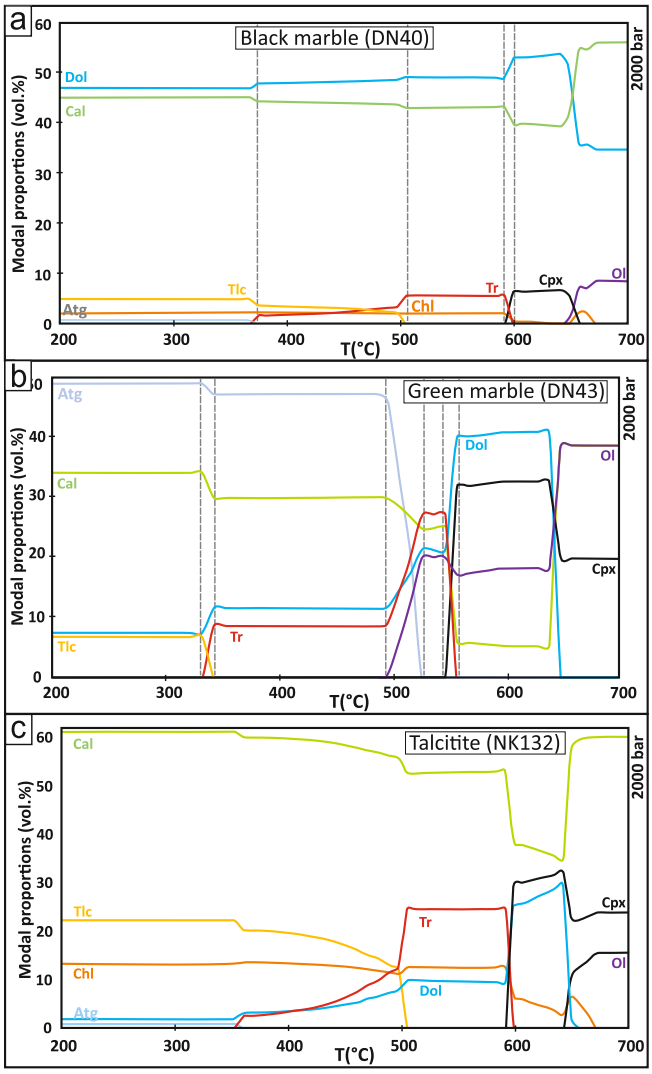

Fig. 15. Modal composition as a function temperature diagram at 2 kbar pressure, showing the evolution of assemblages for the bulk rock composition of: (a) black marble, (b) green marble, (c) talcitite (see text for explanations). (For interpretation of the references to colour in this figure legend, the reader is referred to the web version of this article.)

transformed into chlorite-rich layers (Schärer et al., 1999; de Parseval et al., 2004; Boutin et al., 2016; Boutin, 2016). The source of Mg to form talc was expected to be the proximal exhumed mantle (Moine et al., 1989) but more recent data suggest that, alternatively, it came from proximal dolomitic carbonates (Boutin, 2016).

The Nkob talc deposit remains truly unique in that it hosts a mixture of two types of talc formed by two different processes. Acicular talc 1 formed near the granite after retrogression of acicular tremolite formed bet. Tabular talc formed in the outer aureole by reaction between dolomite and silica-aqueous fluids at temperatures below 350 °C (Figs. 14 and 15). This difference with other deposits is due to the stability of tremolite over diopside in the inner aureole of the Amassine granite. Diopside forms at temperatures above 550–600 °C while tremolite is stable below 550–600 °C (Fig. 14); this observation suggests that temperature in the aureole probably did not exceed 550–600 °C. Second, chlorite is a minor mineral at Nkob compared to other talc-chlorite deposits hosted by metasedimentary rocks. Hydrothermal circulations have not affected aluminous schist as it is the case at Trimouns (de Parseval et al., 2004). Third, it should be noted that one of the main problems of talc deposits worldwide (whether in a carbonate or ultrabasic environment) is the presence of asbestos minerals such as

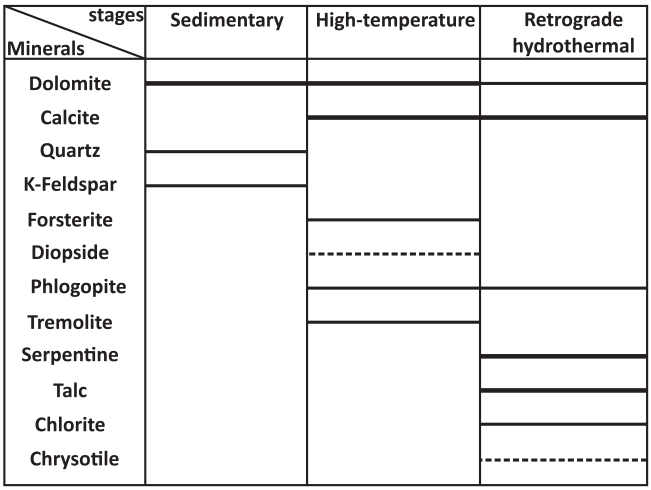

Fig. 16. Simplified paragenetic sequence of the Nkob talc deposit. Line thickness represents the relative abundance of minerals in each stage (thick: major, thin: minor, dotted: accessory).

chrysotile and amphibole mixed with talc (Van Gosen et al., 2004). Amphibole is associated to Talc at Nkob but it is characterized by an acicular or tabular habit. Chrysotile is never mixed to Talc, it is restricted to cm- to dm-thick pure veins near the contact with the granite. Careful mining avoiding areas where chrysotile is present should eliminate the health risks associated with the presence of asbestos minerals

8. Conclusions and perspectives

The Nkob talc deposit formed in the contact aureole of the 614 Ma Amassine Ediacaran granite that intruded the siliceous dolostone and metapelites of the Taghdout Group. Two metamorphic stages were defined for the formation of the deposit: (1) a high temperature stage roughly constrained at T > 450 °C, for which metamorphic markers are only preserved in the northwest part of the deposit in contact with the intrusion, and (2) a low temperature hydrothermal stage that occurred in greenschist facies conditions (<520 °C) and was marked by the interaction with aqueous silica-rich fluids responsible for extensive formation of hydrous minerals including serpentine, talc, tremolite, phlogopite and the talc-calcite association of talcitites. The nature of the contact metamorphic rocks are controlled by P-T conditions, protolith composition but also by fluid-rock interaction. Black marbles represent nearly pure dolostones unaffected by hydrothermal veining while green marbles have been percolated by hydrous silica-rich fluids forming serpentine-rich domains in the dolomitic matrix or in veins. Talcitite precursor is probably a siliceous dolostone that was subsequently enriched in H_2O-SiO_2 through interaction with aqueous fluids. Talc in talcitite ores has two origins: (1) retrogressive breakdown of tremolite in a temperature range between 350 °C and 500 °C (acicular talc - inner contact aureole), and (2) reaction of dolomite with silica-aqueous fluids (or quartz and water) at T < 350 °C (tabular talc - outer contact aureole).

Two major unknowns remain after this first investigation. (1) The precise nature and the origin of the aqueous fluid phase should be determined using extensive study on microthermometry, Raman spectroscopy and LA-ICP-MS on fluid inclusions if some with sufficiently large diameter are found (>30 μm). This will help discriminate if the fluid was exsolved from the cooling granite or sourced from dehydration of the host metapelites and/or decarbonation of dolomites. (2) Although the Nkob deposit formed within the contact aureole of an Ediacaran granite, fluid circulations could have been renewed/revived by Variscan orogeny. This is proposed for some metallic deposits in the Anti-Atlas for which radiometric geochronology sometimes yielded Paleozoic

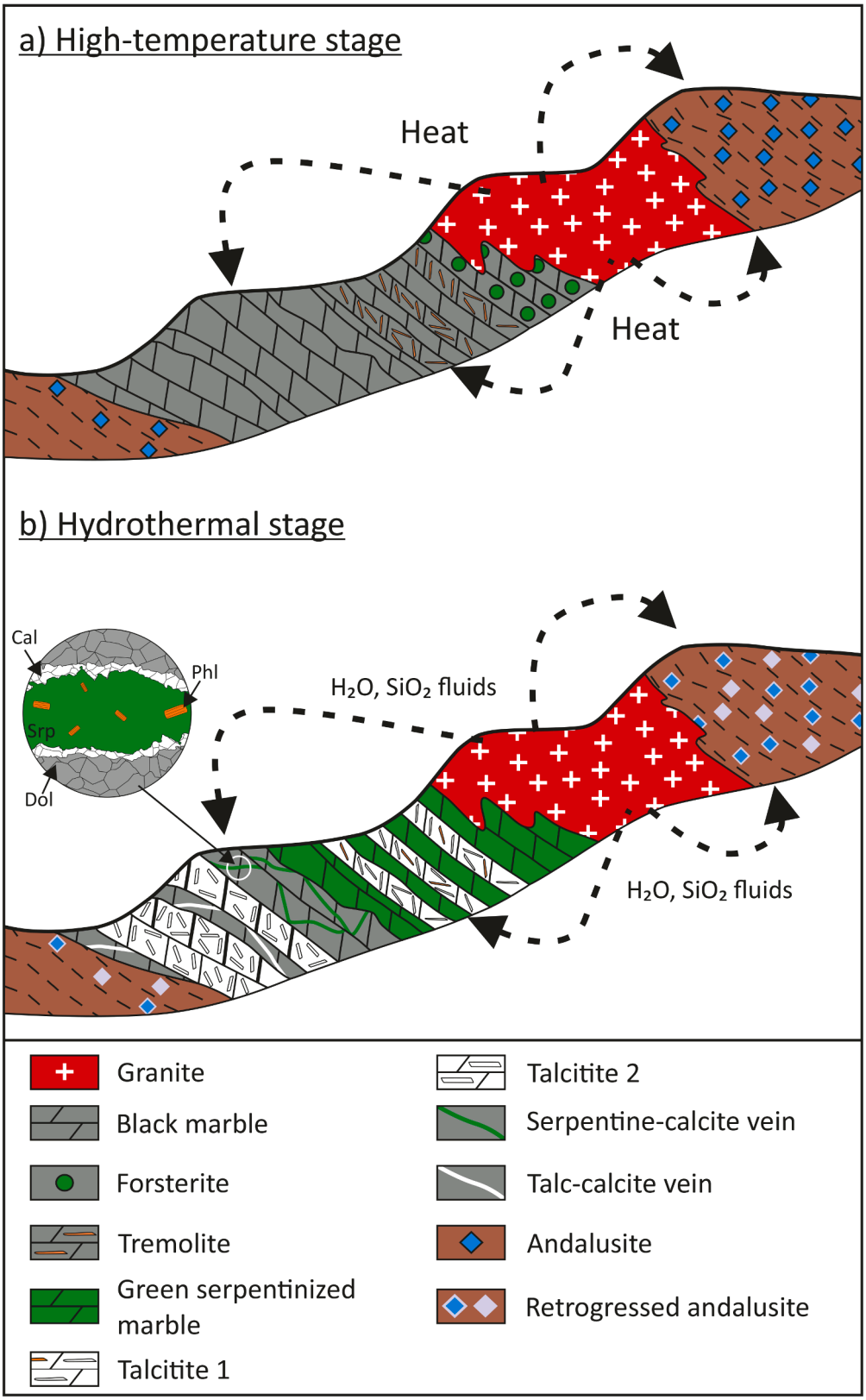

Fig. 17. Conceptual genetic model for talc formation and refinement in the Nkob deposit. a) High temperature stage controlled by heat transfer during granite emplacement. b) Hydrothermal stage controlled by fluid infiltration during granite cooling. The inset show the details of a serpentine vein as found in black-green and green marbles. (For interpretation of the references to colour in this figure legend, the reader is referred to the web version of this article.)

formation or reworking ages. Hence, a thermochronological investigation involving dating with several radiochronological systems characterized by different closure temperatures and variable sensitivity to system opening during fluid circulation will reveal if the Variscan event contributed to a potential reworking of talc at Nkob.

Declaration of Competing Interest

The authors declare that they have no known competing financial interests or personal relationships that could have appeared to influence the work reported in this paper.

Acknowledgements

This research received funding from the PHC TOUBKAL 2019 N° TBK19/90 (CNRST-CNRS bilateral program) and CNRS INSU/TELLUS program through a CESSUR grant. A.T. acknowledges support from the Université Claude Bernard de Lyon with the "*BQR Accueil EC 2021*" and the CLIM-ARC project. Mounir Driss from El Jadida, and Omar from Marrakech are thanked for making thin sections and polished thin sections. Thierry Aigouy helped with SEM observations and Ludovic Menjot provided his expertise in XRD analysis. Fabienne de Parseval has done an exceptional job in making polished thin sections containing talc.

Appendix A. Supplementary data

Supplementary data to this article can be found online at https://doi.org/10.1016/j.oregeorev.2021.104629.

References

Abati, J., Aghzer, A.M., Gerdes, A., Ennih, N., 2010. Detrital zircon ages of Neoproterozoic sequences of the Moroccan Anti-Atlas belt. Prec. Res. 181 (1-4), 115–128. https://doi.org/10.1016/j.precamres.2010.05.018.

Abia et al., 2011. Editions du Service Géologique du Maroc 2011. 9 volumes.

Anderson, D.L., Mogk, D.W., Childs, J.F., 1990. Petrogenesis and timing of talc formation in the Ruby Range, southwestern Montana. Econ. Geol. 85 (3), 585–600. https://doi.org/10.2113/gsecongeo.85.3.585.

Anovitz, L.M., Essene, E.J., 1987. Phase relations in the system CaCO3-MgCO3-FeCO3. J. Petrol. 28, 389–414. https://doi.org/10.1093/petrology/28.2.389.

Blein, O., Baudin, T., Chevremont, P., Soulaimani, A., Admou, H., Gasquet, P., Cocherie, A., Egal, E., Youbi, N., Razin, P., Bouabdelli, M., Gombert, P., 2014. Geochronological constraints on the polycyclic magmatism in the Bou Azzer-El Graara inlier (central Anti-Atlas Morocco). J. Afr. Earth Sci. 99, 287–306. https://doi.org/10.1016/j.jafrearsci.2014.04.021.

Blount, A.M., Vassiliou, A.H., 1980. The mineralogy and origin of the talc deposits near Winterboro. Alabama. Econ. Geol. 75, 107–116. https://doi.org/10.2113/gsecongeo.75.1.107.

Bouougri, E.H., Ait Lahna, A., Tassinari, C.C.G., Basei, M.A.S., Youbi, N., Admou, H., Saquaque, A., Boumehdi, A., Maacha, L., 2020. Time constraints on early Tonian Rifting and Cryogenian Arc terrane-continent convergence along the northern margin of the West African craton: insights from SHRIMP and LA-ICP- MS zircon geochronology in the Pan-African Anti-Atlas belt (Morocco). Gond. Res. 85, 169–188. https://doi.org/10.1016/j.gr.2020.03.011.

Bouougri, E.H., Saquaque, A., 2004. Lithostratigraphic framework and correlation of the Neoproterozoic northern West African Craton passive margin sequence (Siroua-Zenaga-Bouazzer Elgraara inliers, central Anti-Atlas, Morocco): an integrated approach. J. Afr. Earth Sci. 39 (3-5), 227–238. https://doi.org/10.1016/j.jafrearsci.2004.07.045.

Boutin, A., de Saint Blanquat, M., Poujol, M., Boulvais, P., de Parseval, P., Rouleau, C., Robert, J.-F., 2016. Succession of Permian and Mesozoic metasomatic events in the eastern Pyrenees with emphasis on the Trimouns talc–chlorite deposit. Int. J. Earth Sci. 105 (3), 747–770. https://doi.org/10.1007/s00531-015-1223-x.

Boutin, A., 2016. Étude des conditions de formation du gisement de talc–chlorite de Trimouns (Ariège, France). Université de Toulouse. Unpublished PhD thesis.

Bucher, K., Grapes, R., 2011. Petrogenesis of Metamorphic Rocks 8th Edition, Springer. ISBN: 978-3-540-74168-8.

Bucher-Nurminen, K., 1981. The formation of the metasomatic reaction veins in dolomitic marble roof pendants in the Bergell intrusion (Province Sondrio, northern Italy). Am. J. Sci. 281, 1197–1222. https://doi.org/10.2475/ajs.281.9.1197.

Bucher-Nurminen, K., 1988. Compositional variation of phlogopite in a marble sample: implications for geological thermobarometry. J. Metam.Geol. 6, 667–672. https://doi.org/10.1111/j.1525-1314.1988.tb00447.x.

Burkhard, M., Caritg, S., Helg, U., Robert-Charrue, C., Soulaimani, A., 2006. Tectonics of the Anti-Atlas of Morocco. Compt. Rendus Geosci. 338 (1-2), 11–24. https://doi.org/10.1016/j.crte.2005.11.012.

Cahen, L., Snelling, N.J., Delhal, J., Vail, J.R., 1984. The Geochronology and Evolution of Africa. Clarendon Press, Oxford, United Kingdom. p. 512. DOI: 10.1017/S0016756800031666.

Carignan, J., Hild, P., Mevelle, G., Morel, J., Yeghicheyan, D., 2001. Routine analyses of trace elements in geological samples using flow injection and low pressure on-line liquid chromatography coupled to ICP-MS: a study of geochemical reference materials BR, DR-N, UB-N, AN-G and GH. Geostand. Geoanal. Res. 25, 187–198. https://doi.org/10.1111/j.1751-908X.2001.tb00595.x.

Chabu, M., 1995. The Geochemistry Of Phlogopite And Chlorite From The Kipushi Zn-Pb-Cu Deposit, Shaba. Zaire. Can. Mineral. 33, 547–558.

Clauer, N., 1976. Géochimie isotopique du strontium des milieux sédimentaires. Application à la géochronologie du craton ouest-africain. Mem. Sci. Géol. Strasbourg 45, 256 p.

Connolly, J.A.D., 2009. The geodynamic equation of state: What and how. Geochemistry, Geophys. Geosystems 10 (10), n/a–n/a. https://doi.org/10.1029/2009GC002540.

Connolly, J.A.D., 1990. Multivariable phase-diagrams - an algorithm based on generalized thermodynamics. Am. J. Sci. 290 (6), 666–718. https://doi.org/10.2475/ajs.290.6.666.

Cook, S.J., Bowman, J.R., 2000. Mineralogical Evidence for Fluid-Rock Interaction Accompanying Prograde Contact Metamorphism of Siliceous Dolomites: Alta Stock Aureole, Utah, USA. J. Petrol. 41 (6), 739–757. https://doi.org/10.1093/petrology/41.6.739.

de Parseval, P., 1992. Étude minéralogique et géochimique du gisement de talc et chlorite de Trimouns (Thèse de Doctorat). - Paul Sabatier, Université Toulouse III.

de Parseval, P., Jiang, S., Fontan, F., Wang, R., Martin, F., Ferret, J., 2004. Geology and ore genesis of the Trimouns talc chlorite ore deposit. Acta Petrologica Sinica 20 (4), 877–886.

El-Boukhari, A., 1991. Magmatisme et métasédiments associés du Protérozoïque supérieur de la zone de N'Kob (Siroua SE, Anti-Atlas central, Maroc). Une ophiolite formée et mise en place sur la marge du craton ouestafricain. Unpublished thesis, Université Cadi Ayyad, Faculté des Sciences, Marrakech, Maroc, p. 485.

Diener, J.F.A., Powell, R., White, R.W., Holland, T.J.B., 2007. A new thermodynamic model for clino- and orthoamphiboles in the system Na2O–CaO–FeO–MgO–Al2O3–SiO2–H2O–O. J. Metam. Geol. 25, 631–656. https://doi.org/10.1111/j.1525-1314.2007.00720.x.

El-Khanchaoui, T., Lahmam, M., El-Boukhari, A., El-Beraaouz, H., 2001. Les granitoïdes néoprotérozoïques de Khzama, Anti-Atlas central, Maroc: marqueurs de l'évolution d'un magmatisme d'arc à un magmatisme alcaline. J. Afr. Earth Sci. 32 (4), 655–676. https://doi.org/10.1016/S0899-5362(02)00047-7.

El-Sharkawy, M.F., 2000. Talc mineralization of ultramafic affinity in the Eastern Desert of Egypt. Mineral. Dep. 35 (4), 346–363. https://doi.org/10.1007/s001260050246.

Ennih, N., Liégeois, J.-P., 2001. The Moroccan Anti-Atlas: The West African craton passive margin with limited Pan-African activity. Implications for the northern limit of the craton. Precamb. Res. 112, 289–302. https://doi.org/10.1016/S0301-9268(01)00195-4.

Ennih, N., Liégeois, J.P., 2008. The boundaries of the West African craton, with special reference to the basement of the Moroccan metacratonic Anti-Atlas belt. Geol. Soc. Lond., Spec. Pub. 297 (1), 1–17. https://doi.org/10.1144/SP297.1.

Errami, E., Linnemann, U., Hofmann, M., Gärtner, A., Zieger, J., Gärtner, J., Mende, K., El Kabouri, J., Gasquet, D., Ennih, N., 2021. From Pan-African transpression to Cadomian transtension at the West African margin: New U-Pb zircon ages from the Eastern Saghro inlier (Anti-Atlas, Morocco). Geol. Soc. Lond. Spec. Pub. 503 (1), 209–233. https://doi.org/10.1144/SP503-2020-105.

Fuhrman, M.L., Lindsley, D.H., 1988. Ternary feldspar modeling and thermometry. Am. Mineral. 73, 201–215.

Gasquet, D., Ennih, N., Liégeois, J.P., Soulaimani, A., Michard, A., 2008. The Pan-African belt. In: Michard, A., Saddiqi, O., Chalouan, A., Frizon de Lamotte, D. (Eds.), Continental Evolution: The Geology of Morocco. Lecture Notes in Earth Sciences 116. Springer-Verlag, Berlin Heidelberg, pp. 33–64. DOI: 10.1007/978-3-540-77076-3_2.

Gasquet, D., Levresse, G., Cheilletz, A., Azizi-Samir, M.R., Mouttaqi, A., 2005. Contribution to a geodynamic reconstruction of the Anti-Atlas (Morocco) during Pan-African times with the emphasis on inversion tectonics and metallogenic activity at the Precambrian-Cambrian transition. Prec. Res. 140 (3-4), 157–182. https://doi.org/10.1016/j.precamres.2005.06.009.

Greenwood, W., 1998. A mineralogical analysis of fibrous talc. University of Maryland, College Park, p. 162 pp.. Unpublished MSc Thesis.

Hecht, L., Freiberger, R., Gilg, H.A., Grundmann, G., Kostitsyn, Y.A., 1999. Rare earth element and isotope (C, O, Sr) characteristics of hydrothermal carbonates: genetic implications for dolomite hosted talc mineralization at Göpfersgrün (Fichtelgebirge, Germany). Chem. Geol. 155 (1-2), 115–130. https://doi.org/10.1016/S0009-2541(98)00144-2.

Hefferan, K., Soulaimani, A., Samson, S.D., Admou, H., Inglis, J., Saquaque, A., Latifa, C., Heywood, N., 2014. A reconsideration of Pan African orogenic cycle in the Anti-Atlas Mountains, Morocco. J. Afr. Earth Sci. 98, 34–46. https://doi.org/10.1016/j.jafrearsci.2014.03.007.

Hodel, F., Triantafyllou, A., Berger, J., Macouin, M., Baele, J.M., Mattielli, N., Monnier, C., Trindade, R.I.F., Ducea, M.N., Chatir, A., Ennih, N., Langlade, J., Poujol, M., 2020. The Moroccan Anti-Atlas ophiolites : Timing and melting processes in an intra-oceanic arc-back-arc environment Gond. Res. 86, 182–202. https://doi.org/10.1016/j.gr.2020.05.014.

Holland, T.J.B., Powell, R., 1996. Thermodynamics of order–disorder in minerals. Am. Mineral. 81, 1425–1437. https://doi.org/10.2138/am-1996-11-1214.

Holland, T.J.B., Powell, R., 1998. An internally-consistent thermodynamic dataset for phases of petrological interest. J. Metam. Geol. vol. 16 (pg, 309–344. https://doi.org/10.1111/j.1525-1314.1998.00140.x.

Holland, T.J.B., Powell, R., 2011. An improved and extended internally consistent thermodynamic dataset for phases of petrological interest, involving a new equation of state for solids. J. Metam. Geol. 29, 333–383. https://doi.org/10.1111/j.1525-1314.2010.00923.x.

Holness, M.B., 1997. Geochemical self-organization of olivine- grade contact-metamorphosed chert nodules in dolomite marble, Kilchrist. Skye. J. Metam. Geol. 15 (6), 765–775. https://doi.org/10.1111/j.1525-1314.1997.00050.x.

Ikenne, M., Soderlund, U., Ernst, R., Pin, C., Youbi, N., El Aouli, E.H., 2017. A c. 1710 Ma mafic sill emplaced into a quartzite and calcareous series from Igherm, Anti-Atlas, Morocco: evidence that the Taghdout passive margin sedimentary group is nearly 1 Ga older than previously thought. J. Afr. Earth Sci. 127, 113–135. https://doi.org/10.1016/j.jafrearsci.2016.08.020.

Li, C., Wang, R., Lu, X., Zhang, M., 2013. Mineralogical characteristics of unusual black talc ores in Guangfeng County, Jiangxi Province, China. Appli. Clay Sci. 74, 37–46. https://doi.org/10.1016/j.clay.2012.12.004.

Moine, B., Fortune, J.P., Moreau, P., Viguier, F., 1989. Comparative mineralogy, geochemistry and conditions of formation of two metasomatic talc and chlorite deposits: Trimouns (Pyrenees, France) and Rabenwald (Eastern Alps, Austria). Econ. Geol. 84, 1398–1416. https://doi.org/10.2113/gsecongeo.84.5.1398.

Noack, Y., Decarreau, A., Manceau, A., 1986. Spectroscopic and oxygen isotope evidence for low and high temperature origin of talc. Bull. Minéral. 109, 253–263. https://doi.org/10.3406/bulmi.1986.7932.

Noh, J., Kim, C., Samuel, V.O., Jang, Y., Park, S.-I., Kwon, S., 2020. Fluid infiltration and mass transfer along a lamprophyre dyke–marble contact: an example from the south-western Korean peninsula. Minerals 10, 828. https://doi.org/10.3390/min10090828.

Padrón-Navarta, J.A., López Sánchez-Vizcaíno, V., Hermann, J., Connolly, J.A.D., Garrido, C.J., Gómez-Pugnaire, M.T., Marchesi, C., 2013. Tschermak's substitution in antigorite and consequences for phase relations and water liberation in high-grade serpentinites. Lithos 178, 186–196. https://doi.org/10.1016/j.lithos.2013.02.001.

Prochaska, W., 1989. Geochemistry and genesis of Austrian talc deposits. Appl. Geochem. 4 (5), 511–525. https://doi.org/10.1016/0883-2927(89)90008-5.

Prochaska, W., Mogessie, A., Raith, J.G., 1992. Formation of the talc deposit of Kibanda (Rwanda) and its relation to the regional metamorphic evolution. J. Afr. Earth Sci. 14 (4), 499–509. https://doi.org/10.1016/0899-5362(92)90082-N.

Rice, J.M., 1977. Progressive metamorphism of impure dolomitic limestone in the Marysville aureole. Montana. Am. J. Sci. 277 (1), 1–24. https://doi.org/10.1007/BF00374555.

Rieder, M., Cavazzini, G., D'yakonov, Y.S., Frank-Kamenetskii, V.A., Gottardi, G., Guggenheim, S., Koval', P.V., Müller, G., Neiva, A.M.R., Radoslovich, E.W., Robert, J.L., Sassi, F.P., Takeda, H., Weiss, Z., Wones, D.R., 1999. Nomenclature of the micas. Min. Mag. 63, 267–279. https://doi.org/10.1180/minmag.1999.063.2.13.

Samson, S.D., Inglis, J.D., D'Lemos, R.S., Admou, H., Blichert-Toft, J., Hefferan, K., 2004. Geochronological, geochemical, and Nd–Hf isotopic constraints on the origin of Neoproterozoic plagiogranites in the Tasriwine ophiolite, Anti-Atlas orogeny. Morocco. Prec. Res. 135 (1–2), 133–147. https://doi.org/10.1016/j.precamres.2004.08.003.

Schandl, E.S., Gorton, M.P., Sharara, N.A., 2002. Eruptive Rocks, Their Genesis, Composition Classification and Their Reaction to Ore-Deposits, with a Chapter on Meteorites. Nature 34 (3-4), 259–273.

Schandl, E.S., Sharara, N.A., Gorton, M.P., 1999. The origin of the Atshan talc deposit in the Hamata area, eastern desert, Egypt: a geochemical and mineralogical study. Can. Mineral. 37, 1211–1227.

Schärer, U., de Parseval, P., Polvé, M., de Saint Blanquat, M., 1999. Formation of the Trimouns talc-chlorite deposit (Pyrénées) from persistent hydrothermal activity between 112 and 97 Ma. Terra Nova 11, 30–37. https://doi.org/10.1046/j.1365-3121.1999.00224.x.

Shand, S., 1927. On the relations between silica, alumina, and the bases in eruptive rocks, considered as a means of classification. Geol. Mag. 64, 446–449.

Shin, D.B., Lee, I.S., 2002. Carbonate-Hosted Talc Deposits in the Contact Aureole of Igneous Intrusion (Hwanggangri Mineralized Zone, South Korea): geochemistry, phase relationships, and stable isotope studies. Ore Geol. Rev. 22, 17–39. https://doi.org/10.1016/S0169-1368(02)00085-9.

Simandl, G.J., Ogden, D., 1999. Ultramafic-hosted talc-magnesite. In: Simandl, G.J., Hora, Z.D., Lefebure, D.V. (Eds.), Selected British Columbia mineral deposit profiles, V. 3. Industrial Minerals, British Columbia Ministry of Energy and Mines.

Sinaei-Esfahani, F., 2013. Localized metasomatism of Grenvillian marble leading to its melting, Autoroute 5 near Old Chelsea, Quebec. McGill University, Montreal, Canada. Sc. thesis.

Skippen, G., 1971. Experimental data for reactions in siliceous marbles. J. Geol. 79 (4), 457–481. https://doi.org/10.2307/30063061.

Soulaimani, A., Ouanaimi, H., Saddiqi, O., Baidder, L., Michard, A., 2018. The Anti-Atlas Pan-African Belt (Morocco): Overview and pending questions. Comptes Rendus Geosci. 350, 279–288. https://doi.org/10.1016/j.crte.2018.07.002.

Tahir, M., Imai, A., Takahashi, R., Yano, S., 2018. Ore genesis and geochemical characteristics of carbonate-hosted talc deposits in nangarhar province. Afghanistan. Res. Geol. 68 (4), 352–372. https://doi.org/10.1111/rge.12174.

Tesalina, S.G., Nimis, P., Augé, T., Zaykov, V.V., 2003. Origin of chromite in mafic–ultramafic-hosted hydrothermal massive sulfides from the Main Uralian Fault, South Urals, Russia. Lithos 70 (1-2), 39–59. https://doi.org/10.1016/S0024-4937(03)00090-2.

Thomas, R.J., Chevallier, L.P., Gresse, P.G., Harmer, R.E., Eglington, B.M., Armstrong, R. A., de Beer, C.H., Martini, J.E.J., de Kock, G.S., Macey, P.H., Ingram, B.A., 2002. Precambrian evolution of the Sirwa window, anti-atlas orogen, Morocco. Prec. Res. 118 (1-2), 1–57. https://doi.org/10.1016/S0301-9268(02)00075-X.

Thomas, R.J., Fekkak, A., Ennih, N., Errami, E., Loughlin, S.C., Gresse, P.G., Chevakier, L. P., Liegeois, J.P., 2004. A new lithostratigraphic framwork for the Anti-Atlas Orogen. Morocco. J. Afr. Earth Sci. 39, 217–226. https://doi.org/10.1016/j.jafrearsci.2004.07.046.

Tornos, F., Spiro, B.F., 2000. The geology and isotope geochemistry of the talc deposits of Puebla de Lillo (Cantabrian Zone, Northern Spain). Econ. Geol. 95 (6), 1277–1296. https://doi.org/10.2113/gsecongeo.95.6.1277.

Tosca, N.J., Macdonald, F.A., Strauss, J.V., Johnston, D.T., Andrew, H.K., 2011. Sedimentary talc in neoproterozoic carbonate successions. Earth Planet. Sci. Lett. 306 (1–2), 11–22. https://doi.org/10.1016/j.epsl.2011.03.041.

Toummite, A., Liegeois, J.P., Gasquet, D., Bruguier, O., Beraaouz, E.H., Ikenne, M., 2013. Field, geochemistry and Sr-Nd isotopes of the Pan-African granitoids from the Tifnoute Valley (Sirwa, Anti-Atlas, Morocco): a post-collisional event in a metacratonic setting. Mineral. Petrol. 107 (5), 739–763. https://doi.org/10.1007/s00710-012-0245-3.

Triantafyllou, A., Berger, J., Baele, J.M., Diot, H., Ennih, N., Plissart, G., Monnier, C., Watlet, A., Bruguier, O., Spagna, P., Vandycke, S., 2016. The Tachakoucht–Iriri–Tourtit arc complex (Moroccan Anti-Atlas): Neoproterozoic records of polyphased subduction-accretion dynamics during the Pan-African orogeny. J Geodyn. 96, 81–103. https://doi.org/10.1016/j.jog.2015.07.004.

Triantafyllou, A., Berger, J., Baele, J.M., Bruguier, O., Diot, H., Ennih, N., Monnier, C., Plissart, G., Vandycke, S., Watlet, A., 2018. Intra-oceanic arc growth driven by magmatic and tectonic processes recorded in the Neoproterozoic Bougmane arc complex (Anti-Atlas, Morocco). Prec. Res. 304, 39–63. https://doi.org/10.1016/j.precamres.2017.10.022.

Triantafyllou, A., Berger, J., Baele, J.-M., Mattielli, N., Ducea, M.N., Sterckx, S., Samson, S., Hodel, F., Ennih, N., 2020. Episodic magmatism during the growth of a Neoproterozoic oceanic arc (Anti-Atlas, Morocco). Prec. Res. 339, 105610. https://doi.org/10.1016/j.precamres.2020.105610.

Tuduri, J., Chauvet, A., Barbanson, L., Bourdier, J.-L., Labriki, M., Ennaciri, A., Badra, L., Dubois, M., Ennaciri-Leloix, C., Sizaret, S., Maacha, L., 2018. The Jbel Saghro Au (–Ag, Cu) and Ag–Hg Metallogenetic Province: Product of a Long-Lived Ediacaran Tectono-Magmatic Evolution in the Moroccan Anti-Atlas. Minerals 8, 592. https://doi.org/10.3390/min8120592.

Van Gosen, B.S., Lowers, H.A., Sutley, S.J., Gent, C.A., 2004. Using the geologic setting of talc deposits as an indicator of amphibole asbestos content. Environ Geol. 45 (7), 920–939. https://doi.org/10.1007/s00254-003-0955-2.

Waldbaum, D.R., Thompson Jr., J.B., 1968. Mixing properries of sanidine crystalline solutions: II. Calculations based on volume data. Am. Miner. 53, 2000–2017.

White, R.W., Powell, R., Holland, T.J.B., Johnson, T.E., Green, E.C.R., 2014. New mineral activity–composition relations for thermodynamic calculations in metapelitic systems. J. Metam. Geol. 32 (3), 261–286. https://doi.org/10.1111/jmg.12071.

White, R.W., Powell, R., Holland, T.J.B., 2001. Calculation of partial melting equilibria in the system Na2O–CaO–K2O–FeO–MgO–Al2O3–SiO2–H2O (NCKFMASH). J. Metam. Geol. 19, 139–153. https://doi.org/10.1046/j.0263-4929.2000.00303.x.

Walsh, G.J., Benziane, F., Aleinikoff, J.N., Harisson, R.W., Yazidi, A., Burton, W.C., Quick, J.E., Saadane, A., 2012. Neoproterozoic tectonic evolution of the Jebel Saghro and BouAzzer-El Graara inliers, eastern and central Anti-Atlas. Morocco. Prec. Res. 216–219, 23–62. https://doi.org/10.1016/j.precamres.2012.06.010.

Whitney, D.L., Evans, B.W., 2010. Abbreviations for Names of Rock-Forming Minerals. Am. Mineral. 95 (1), 185–187. https://doi.org/10.2138/am.2010.3371.

Wölfler, A., Prochaska, W., Fritz, H., 2015. Shear zone related talc mineralizations in the Veitsch nappe of the eastern Greywacke Zone (Eastern Alps, Austria). Aus. J. Earth Sci. 108 (1), 50–72. https://doi.org/10.17738/ajes.2015.0004.

Yalçin, H., Bozkaya, Ö., 2006. Mineralogy and geochemistry of ultramafic- and sedimentary-hosted talc deposits of Paleocene in the southern part of the Sivas basin. Turkey. Clays. Clay. Miner. 54, 333–350. https://doi.org/10.1346/CCMN.2006.0540305.

Yau, K.-W., Nakatani, K., 1984. Electrogenic Na–Ca exchange in retinal rod outer segment. Nature 311 (5987), 661–663. https://doi.org/10.1038/311661a0.

Youbi, N., Kouyaté, D., Söderlund, U., Ernst, R., Soulaimani, A., Hafid, A., Ikenne, M., El Bahat, A., Bertrand, H., Rkha Chaham, K., Ben Abbou, M., Mortaji, A., El Ghorfi, M., Zouhair, M., El Janati, M., 2013. The 1750 Ma Magmatic Event of the West African Craton (Anti-Atlas, Morocco). Prec. Res. 236, 106–123. https://doi.org/10.1016/j.precamres.2013.07.003.